HIGHER ORDER TURBULENCE CLOSURE MODELS

by

Ryoichi S. Amano

Principal Investigator

John C. Chai and Jau-Der Chen

Research Assistants

Department of Mechanical Engineering

The University of Wisconsi-Milwaukee

Milwaukee, Wisconsin 53201

v

Abstract

Theoretical models are developed and numerical studies are conducted on various types of flows including both elliptic and parabolic flows. The purpose of this study is to find better higher order closure models for the computations of complex flows.

This report summarizes three new achievements: i) Completion of the Reynolds-stress closure by developing a new pressure-strain correlation, ii) development of a parabolic code to compute jets and wakes, and iii) application to a flow through $180°$ turn around duct by adopting a boundary fitted coordinate system.

In the above mentioned models near-wall models are developed for the pressure-strain correlation model and third-moment, and incorporated into the transport equations. This addition improved the results considerably and is recommended for future computations.

A new parabolic code to solve shear flows without coordinate transformations is developed and incorporated in this study. This code uses the structure of the finite volume method to solve the governing equations implicitly. The code was validated with the experimental results available in literature.

Acknowledgements

Nomenclature

a	coefficient in the discretization equation
a_{ij}	anisotropy
b	source or sink in discretization equation
$A(\lvert P \rvert)$	A-function for differencing schemes
C_{ϕ_1}, C_{ϕ_2}	constants used in the Reynolds Stresses pressure-strain correlations
C_1, C_2	constants used in the source terms of the turbulent energy dissipations
C_γ	constant used in $\phi_{ijk,T}$ of $< u_i u_j u_k >$
$C_{\gamma w}$	wall constant used in $\phi_{ijk,T}$ of $< u_i u_j u_k >$
C_μ	constant used in calculation of turbulent eddy viscosity
$C_{\varepsilon\gamma}$	coefficient for the dissipation rate of $< u_i u_j u_k >$
$C_{\theta\gamma}$	constant used in $< \phi_{ij\theta} >$ of $< u_i u_j \theta >$
$C_{\theta\varepsilon}$	constant used in $\varepsilon_{ij\theta}$ of $< u_i u_j \theta >$
C_{1T}, C_{2T}	Constants used in algebraic equations of $< u_i \theta >$ of Launder and Samaraweera
C_g	constant used in P_{ijk_1} of $< u_i u_j u_k >$
$C_{i\theta,1}, C_{i\theta,2}$	constants used in $\phi_{i\theta}$ of $< u_i \theta >$
C_{ij}	constants used in boundary conditions of $< u_i u_j >$
C_f	skin friction coefficient, $= \frac{\tau_w}{\frac{1}{2}\rho U_{IN}^2}$
C_l	constant used in the near wall model of $< u_i u_j u_k >$, $= \kappa C_\mu^{-\frac{3}{4}}$
C_p	wall static pressure coefficient, $= \frac{P - P_{ref}}{\frac{1}{2}\rho U_{IN}^2}$
C_P	constant pressure heat capacity
C_s	constant used in diffusion rate of $< u_i u_j >$
C_{t1}, C_{t2}	Temporary constants used in term IV of $< u_i u_j \theta >$
d	nozzle diameter

$D_{i\theta}$	diffusion rate of $<u_i\theta>$
D_{ij}	diffusion rate of $<u_iu_j>$
$D_{ij\theta}$	diffusion rate of $<u_iu_j\theta>$
D_{ijk}	diffusion rate of $<u_iu_ju_k>$
D_c	height of channel downstream of the step, $=(Y_0+H)$
G	generation rate of turbulent kinetic energy
G_{ij}	primary generation or production rate of $<u_iu_j>$
H	step height of backward-facing step
H_{ij}	secondary generation or production rate of $<u_iu_j>$
i	turbulence intensity
k	turbulent kinetic energy
l_m	mixing length
p	pressure fluctuation
P	mean pressure
P_i	cell Peclet number
$P_{i\theta}$	production rate of $<u_i\theta>$
$P_{ij\theta,1}$	generation or production rate of $<u_iu_j\theta>$ due to mean strain rate
$P_{ij\theta,2}$	generation or production rate of $<u_iu_j\theta>$ due to interactions between Reynolds stresses and second moments of velocity-temperature products
P_{ijk_1}	generation or production rate of $<u_iu_ju_k>$ due to mean strain rate
P_{ijk_2}	generation or production rate of $<u_iu_ju_k>$ due to interactions between the Reynolds stresses and their gradients
Pr	Prandtl number
Pr_t	turbulent Prandtl number
$\dot{q}''_w$	wall heat flux per unit width
r_N	radius of the nozzle
Re_d	orifice Reynolds number, $=\frac{U_{in}d}{\nu}$
Re_H	step-height Reynolds number, $=\frac{U_{in}H}{\nu}$
S_ϕ	source terms of transport equations in the discretization equation, $=S_U+S_P\phi_P$
S_U, S_P	linearized source terms in S_ϕ
T	mean temperature

T_{IN}	inlet stream velocity
T_m	Maximum temperature in shear layer
T_w	local wall temperature
u	fluctuating velocity in x-direction
$< u_i\theta >$	second moments of temperature-velocity products
$< uu >$	axial component of $< u_iu_j >$
$< uv >$	Reynolds shear stress
$< u_iu_j >$	Reynolds Stresses
$< u_iu_j\theta >$	third moments of velocity-temperature products
$< u_iu_ju_k >$	hydrodynamics third moments of turbulence
U	mean velocity in x-direction
U_τ	friction velocity
U_i	mean velocity components
U_0	discharge velocity in coflowing jets
U_{IN}	inlet velocity
U_m	Maximum velocity in shear layer
U_s	surrounding velocity in coflowing jets
v	fluctuating velocity in y-direction
$< vv >$	transverse component of $< u_iu_j >$
V	mean velocity in y-direction
x,y	cartesian coordinates
x'	normalized coordinate, $= \frac{(x-x_R)}{x_R}$
x_n	normal distance from the wall
x_R	reattachment length measured from the step
$y_{\frac{1}{2}\theta}$	half-maximum temperature width
$y_{\frac{1}{2}u}$	half-maximum velocity width
y_1	coordinate normal to the wall
y_2	coordinate parallel to the wall
Y_0	channel width upstream of step

GREEK SYMBOLS

α	thermal diffusivity

δ_{ij}	kronecker delta
ε	dissipation rate of turbulent kinetic energy
$\varepsilon_{i\theta}$	dissipation rate of $< u_i\theta >$
ε_{ij}	dissipation rate of $< u_i u_j >$
$\varepsilon_{ij\theta}$	dissipation rate of $< u_i u_j\theta >$
ε_{ijk}	dissipation rate of $< u_i u_j u_k >$
η_θ	similarity coordinate for temperature in shear layer, $= \frac{y}{y_{\frac{1}{2}\theta}}$
η_u	similarity coordinate for velocity in shear layer, $= \frac{y}{y_{\frac{1}{2}u}}$
Γ	diffusion coefficient in general governing and discretization equations of parabolic equation
Γ_1, Γ_2	diffusion coefficients in x- and y-direction in general governing and discretization equations of elliptic equation
κ	Von-Karman constant
λ	length-scale constant
ν	kinematic viscosity
ν_{eff}	effective kinematic viscosity, $= \nu + \nu_t$
ν_t	kinematic eddy viscosity
ϕ	dependent variables in general governing and discretization equations
$\phi_{i\theta}$	pressure-heat flux effects of $< u_i\theta >$
$\phi_{i\theta,w}$	wall correction of pressure-heat flux effects of $< u_i\theta >$
ϕ_{ij}	pressure-strain correlations of $< u_i u_j >$
$\phi_{ij,1}$	pressure-strain correlations of $< u_i u_j >$ due to fluctuating components
$\phi_{ij\theta}$	pressure-heat flux effects of $< u_i u_j\theta >$
ϕ_{ijk}	pressure-strain correlations of $< u_i u_j u_k >$
$\phi_{ijk,T}$	total pressure-strain correlations of $< u_i u_j u_k >$, $= \phi_{ijk} + \phi_{ijk,w}$
$\phi_{ijk,w}$	near-wall low-Reynolds number pressure-strain correlations of $< u_i u_j u_k >$
ρ	density of fluid
σ_k	turbulent Prandtl number for k
σ_ε	turbulent Prandtl number for ε, $= \frac{\kappa C_\mu^{-\frac{1}{2}}}{C_2 - C_1}$
τ	shear stress
θ	fluctuating temperature

SUBSCRIPTS

i,j,k,l	tensor notations
E,W,N,S	nodes at east,west,north and south of cell P
IN	inlet station conditions
P	node cell P
R	reattachment station conditions
e,w,n,s	cell boundaries at east, west, north and south of cell P
ref	reference station ($x/\mathrm{H} = -4$) conditions
w	wall values

SYMBOLS

$<>$	time-averaged values
$\parallel A, B, C, ... \parallel$	maximum of A, B, C, ...

Contents

List of Tables

List of Figures

Chapter 1

Introduction

In the past decade, Computational Fluid Dynamics (CFD) is assuming an important role in design with the advancements in computer technology and numerical method. Peterson and Bailey [1] cited that supercomputers are becoming so powerful that aerodynamic flow simulations are almost as good as wind tunnel testing. It was noted that the sophistication of computational fluid dynamics is so advanced that results of computed surface pressure on the shuttle launch configuration with Mach number 1.55 and Reynolds number of 2.5×10^6 coincided with a wind tunnel testing and flight data.

Most commercial firms and research institutes use the conventional $k - \varepsilon$ model of turbulence which gives satisfactory results for planar, wall-shear layer and favorable pressure gradient internal flows. This model uses the eddy viscosity concept assuming that turbulence is locally isotropic or the normal components of the Reynolds stresses have equal magnitudes in all directions. However, in flow fields where large rates of strain are imposed by curvature, sharp corner, swirl and body forces, the magnitudes of Reynolds stresses are no longer equal in all directions. Thus, the isotropic assumption of the $k - \varepsilon$ model fails to give realistic results. Driver and Seegmiller [2] pointed out that the $k - \varepsilon$ model of Jones and Launder [3] overestimated the isotropic turbulent viscosity in recirculating flows resulting a higher spreading rate for the shear layer giving a premature reattachment.

The next attractive alternative to correct this problem is to use the algebraic stress models (ASM) which are approximations of the full transport equations of the

Reynolds stresses in algebraic form. Hutchings and Iannuzzelli [4] reported compu-
tations of highly swirling flow with the $k - \varepsilon$ model and the algebraic stress model
and illustrated the deficiency of the $k - \varepsilon$ model in the predictions of swirling flows.
The disadvantage of using the algebraic stress model is that it does not take the
convective and diffusive transport of Reynolds stresses into considerations. In high
Reynolds number flows, the convective processes play an important role and should
not be omitted in the computations.

1.1   Literature Survey

Chandrsuda and Bradshaw [5] carried out the experiment with a step-height
Reynolds number of about 10^5, a step height of 51 mm, inlet nozzle of 127 mm and
inlet freestream velocity of 31.5 m/s. The reattachment point was found from surface
oil-flow measurements to be about 5.9 step heights downstream of the step. Hot-wire
and pressure-probe were used to measure the important quantities, while the skin-
friction coefficient was obtained from surface tube measurements. Although there
were no specific number given for the uncertainties of measurements, measurements
inside the recirculation zone were recommended for quantitative use only.

Driver and Seegmiller [6] conducted the experiment with a step-height Reynolds
number of 3.78×10^4, a step-height of 1.27 cm, inlet nozzle of 10.16 cm and freestream
inlet velocity of 44.2 m/s. The reattachment point was found to be 6.2 step heights
downstream of the step. The uncertainty of the measured wall static pressure coeffi-
cient and skin-friction coefficient were $\pm$ 0.0009 and $\pm$ 8% ($\pm$ 15 % in the separated
region of the flow) respectively. No uncertainty values were reported for other quan-
tities.

Eaton and Vogel [7] performed the experiment with a constant heat-flux surface
behind a single-sided backward-facing step . It was conducted with a step-height
Reynolds number of 28000, a step height of 3.8 cm, freestream inlet velocity of 11.3
m/s and constant heat flux of 270 W/m. The uncertainties of the heat flux, mean ve-
locity, and fluctuating velocity were 1% , 1% and 2%, respectively. The reattachment
point was $6\frac{2}{3}$ step heights downstream of the step.

Figure 1 shows the experimental conditions for all three experiments.
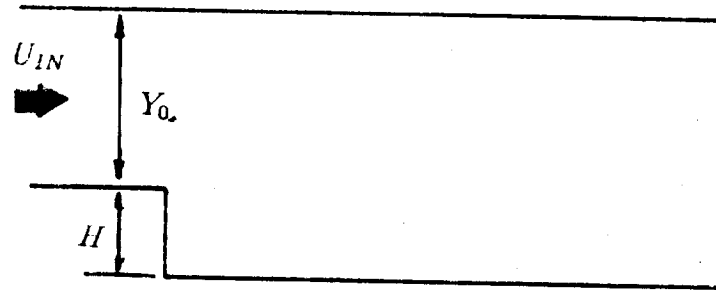
(a) Chandrsuda and Bradshaw

$$H \quad = 57\,mm$$
$$Y_0 \quad = 127\,mm$$
$$U_{IN} \quad = 31.5\,m/s$$
$$Re_H \quad = 10^5$$
$$x_R \quad = 5.9\,H$$

(b) Driver and Seegmiller

$$H \quad = 1.27\,cm$$
$$Y_0 \quad = 10.16\,cm$$
$$U_{IN} \quad = 44.2\,m/s$$
$$Re_H \quad = 3.78 \times 10^4$$
$$x_R \quad = 6.2\,H$$

(c) Eaton and Vogel

$$H \quad = 3.8\,cm$$
$$Y_0 \quad = 15\,cm$$
$$U_{IN} \quad = 11.3\,m/s$$
$$(q)''_w \quad = 270\,W/m$$
$$Re_H \quad = 28000$$
$$x_R \quad = 6\tfrac{2}{3}\,H$$

Figure 1: Experimental conditions for all three backward-facing step experiments investigated

Antonia et al. [8, 9, 10, 11, 12, 13] conducted the experiment with a variable-speed centrifugal squirrel cage blower which supplies air to a setting chamber followed by a vertical nozzle of contraction ratio 20:1. The nozzle exit velocity was 9 m/s, orifice Reynolds number, Re_d, was 7550 and jet temperature was maintained at a nominal temperature of 25^0C relative to the ambient temperature. Measurements for mean velocity and temperature were done using a 5 μm hot wire with a DISA 55M01 constant temperature anemometer and a 0.63 μm cold wire drawing 0.1 mA in a constant current circuit. Fluctuating temperatures were measured with cold wires operated at very low overheat as resistance thermometers in constant current circuits.

Heskestad [14] performed the experiment by exhausting a constant velocity jet into still air. The exit nozzle velocity and orifice Reynolds number were 1.27 cm and 3.4×10^4, respectively. Hot wire was used to measure all quantities and true self-preservation was not attained [15].

Gutmark and Wygnanski [16] measured mean velocities, turbulence intensities, third- and fourth-moment, as well as, two-point correlations and the intermittency factor by hot wire. Measurements were made up to a distance of $x/d = 120$ and flow was found to be self-preserving beyond $x/d = 40$. The exhaust velocity, orifice Reynolds number and exit nozzle width were $35 m/s$, 3×10^4 and $1.3 cm$, respectively.

Everitt and Robins [15] performed an experiment on submerged jet with a variable nozzle width ranging from 0.32 cm to 2.54 cm. Documentations were made on the Reynolds stresses and triple-moment products of velocities.

Wygnanski and Fiedler [17, 18] found that most previous investigators did not measure the turbulent quantities far downstream enough to ensure self-preservation was achieved. Measurements were made beyond 100 nozzle diameters by the authors to ensure self-preservation conditions were attained

Numerical studies of separating and reattaching flows are less numerous than experimental studies. During the sixties, Gosman et al. [19] pioneered the theoretical work on turbulent flows predictions. Pope and Whitelaw [20] studied the near wake flows using three different models of turbulence.

Schlichting [21] attacked the problem of plane laminar jet and computed the velocity across the jet by an approximate numerical method from the fundamental equations of constant density viscous flow. In going through Schlichting's work, Bickley [22] and Goldstein [23] found that in a plane jet case, the equations are integrable

in close form.

In the past few years, increase attentions have been given to the development of second-order turbulence models. This is the simplest closure level which can incorporate the essential turbulent flow characteristics such as transport, pressure-interactions, dissipations and effects of external force fields.

Hanjalic and Launder [24] performed computational works on a plane mixing layer, plane jet, boundary layer and channel flow by using second-moment turbulence closure. Dekeyser [25] computed an asymmetrically heated coflowing plane jet with second-moment closure. Sini and Dekeyser [26, 27] performed numerical work on turbulent shear flows using second-moment turbulence closure and on turbulent plane jets and forced plumes using the $k - \varepsilon$ model of turbulence, respectively. Dekeyser and Launder [28] modeled the triple moments of velocity and velocity-temperature of a coflowing jet. Samaraweera [29] documented numerical results of two and three dimensional temperature field and later combined with Launder [30] to apply second-moment turbulence closure to investigate heat and mass transport in thin shear flows.

All computations were performed by using the computer code of Patankar and Spalding [31] with some minor modifications of staggering the $< uv >$ cell.

1.2 Objectives

The objectives of this study are listed below :

1. Refine the existing Reynolds stresses and third-moment turbulent computations.

2. Develop a new parabolic code for the computations of parabolic flows without coordinate transformations

3. Apply the above formulations to a 180° turn around duct flows by using a boundary fitted coordinates.

Chapter 2

Mathematical Formulations

This chapter defines all the transport and algebraic equations governing the dependent variables used in this study.

2.1 Transport Equations

Reynolds-Stress Equations

$$U_k \frac{\partial < u_i u_j >}{\partial x_k} = G_{ij} - \varepsilon_{ij} + \phi_{ij} + D_{ij} \tag{1}$$

where

$$
\begin{aligned}
G_{ij} &= - \left(< u_j u_k > \frac{\partial U_i}{\partial x_k} + < u_i u_k > \frac{\partial U_j}{\partial x_k} \right) \\
D_{ij} &= C_s \frac{\partial}{\partial x_k} \left[\frac{k}{\varepsilon} < u_k u_l > \frac{\partial < u_i u_j >}{\partial x_l} \right] \\
\varepsilon_{ij} &= \frac{2}{3} \delta_{ij} \varepsilon
\end{aligned}
$$

There are a few models for ϕ_{ij}

Model 1 : Naot et al. [34]:

$$\phi_{ij} = -C_{\phi_2} \left(G_{ij} - \frac{2}{3} \delta_{ij} G \right) + \phi_{ij,1} \tag{2}$$

Model 2 : Amano et al:(see section 2.3)

$$\phi_{ij} = (7C_{\phi_2} - 10)G\left(\frac{<u_i u_j>}{k} - \frac{2}{3}\delta_{ij}\right) - \frac{2}{5}(2C_{\phi_2} - 1)k\left(\frac{\partial U_i}{\partial x_j} + \frac{\partial U_j}{\partial x_i}\right)$$

$$-2(C_{\phi_2} - 1)\left(G_{ij} - \frac{2}{3}\delta_{ij}G\right) - 2(C_{\phi_2} - 1)\left(H_{ij} - \frac{2}{3}\delta_{ij}G\right) + \phi_{ij,1} \qquad (3)$$

Model 3 : Launder et al: [36]:

$$\phi_{ij} = -\frac{(C_{\phi_2} + 8)}{11}\left(G_{ij} - \frac{2}{3}\delta_{ij}G\right) - \frac{(8C_{\phi_2} - 2)}{11}\left(H_{ij} - \frac{2}{3}\delta_{ij}G\right)$$

$$-\frac{(30C_{\phi_2} - 2)}{55}k\left(\frac{\partial U_i}{\partial x_j} + \frac{\partial U_j}{\partial x_i}\right) + \phi_{ij,1} \qquad (4)$$

where

$$H_{ij} = -\left(<u_i u_k>\frac{\partial U_k}{\partial x_j} + <u_j u_k>\frac{\partial U_k}{\partial x_i}\right)$$

$$G_{ij} = -\left(<u_j u_k>\frac{\partial U_i}{\partial x_k} + <u_i u_k>\frac{\partial U_j}{\partial x_k}\right)$$

$$\phi_{ij,1} = -C_{\phi_1}\frac{\varepsilon}{k}\left(<u_i u_j> - \frac{2}{3}\delta_{ij}k\right) \qquad (5)$$

$$G = -<u_i u_j>\frac{\partial U_i}{\partial x_j}$$

<u>Third-Moment Equations:</u> Low-Reynolds number model [37]:

$$U_l\frac{\partial}{\partial x_l}(<u_i u_j u_k>) = P_{ijk_1} + P_{ijk_2} + \underbrace{\phi_{ijk} + \phi_{ijk,w}}_{\phi_{ijk,T}} - \varepsilon_{ijk} + D_{ijk} \qquad (6)$$

where

$$P_{ijk_1} = -C_g\left(<u_i u_j u_l>\frac{\partial U_k}{\partial x_l} + <u_j u_k u_l>\frac{\partial U_i}{\partial x_l} + <u_k u_i u_l>\frac{\partial U_j}{\partial x_l}\right)$$

$$P_{ijk_2} = -\left(<u_k u_l>\frac{\partial<u_i u_j>}{\partial x_l} + <u_i u_l>\frac{\partial<u_j u_k>}{\partial x_l} + <u_j u_l>\frac{\partial<u_k u_i>}{\partial x_l}\right)$$

$$\phi_{ijk,T} = -C_\gamma\frac{<u_i u_j u_k>}{k}\parallel \varepsilon, C_{\gamma w}\frac{k^{\frac{3}{2}}}{C_l x_n}, 2\nu\left(\frac{\partial k^{\frac{1}{2}}}{\partial y}\right)^2 \parallel$$

$$\varepsilon_{ijk} = C_{\varepsilon\gamma}\varepsilon k^{\frac{1}{2}}$$

$$D_{ijk} = \frac{\partial}{\partial x_l}\left(\nu\frac{\partial}{\partial x_l}<u_i u_j u_k>\right)$$

High-Reynolds number model:

$$\phi_{ijk,T} = -C_\gamma\frac{<u_i u_j u_k>}{k}\varepsilon$$

$$\varepsilon_{ijk} = 0.0$$

2.2 Heat Transfer Governing Equations

2.2.1 Scalar Double Product Equations

The transport equations of second moments of velocity-temperature, $< u_i\theta >$, are formulated and simplified through closures. After neglecting insignificant terms, the transport equations reduce to the following [38]:

$$U_j\frac{\partial}{\partial x_j}(< u_i\theta >) = \underbrace{-\left[< u_iu_j > \frac{\partial T}{\partial x_j} + < u_j\theta > \frac{\partial U_i}{\partial x_j}\right]}_{I}$$
$$\underbrace{+\frac{\partial}{\partial x_j}\left[(\alpha + \nu)\frac{\partial < u_i\theta >}{\partial x_j} - < u_iu_j\theta >\right]}_{II}$$
$$\underbrace{+ < \frac{p}{\rho}\frac{\partial\theta}{\partial x_i} >}_{III} \underbrace{-(\alpha + \nu) < \frac{\partial\theta}{\partial x_j}\frac{\partial u_i}{\partial x_j} >}_{IV} \tag{7}$$

which can be written as

$$U_j\frac{\partial}{\partial x_j}(< u_i\theta >) = P_{i\theta} + D_{i\theta} + \phi_{i\theta} + \phi_{i\theta,w} - \varepsilon_{i\theta} \tag{8}$$

where

$P_{i\theta}$	= Production rate of $< u_i\theta >$. (Term I)
$D_{i\theta}$	= Diffusion rate of $< u_i\theta >$. (Term II)
$\phi_{i\theta}$	= Pressure-heat flux effects. (Term III)
$\phi_{i\theta,w}$	= Wall correction of pressure-heat flux. (Term III)
$\varepsilon_{i\theta}$	= Dissipation of $< u_i\theta >$. (Term IV)

Term I is explicit in character and thus needs no further modifications. The diffusive rates, which is term II contains the triple products $< u_iu_j\theta >$ which has to be closed by using an appropriate closure, is decomposed into simpler form following Launder's procedure [39].

$$< u_iu_j\theta >= -0.15(2\frac{k}{\varepsilon}) < u_ju_l > \frac{\partial < u_i\theta >}{\partial x_l} \tag{9}$$

The pressure-heat flux effects can be modeled as follow [39].

$$\phi_{i\theta} = -C_{i\theta,1}\frac{\varepsilon}{k} < u_i\theta > +C_{i\theta,2} < u_l\theta > \frac{\partial U_i}{\partial x_l} \tag{10}$$

The near-wall correction of pressure-heat flux effect is proposed by Launder and Samaraweera [30] as

$$\phi_{i\theta,w} = \left[-0.1\frac{\varepsilon}{k} < u_i\theta > -0.02 < u_l\theta > \left(4\frac{\partial U_i}{\partial x_l} - \frac{\partial U_l}{\partial x_i}\right)\right]\frac{k^{\frac{3}{2}}}{\varepsilon x_n} \qquad (11)$$

The dissipation rate is assumed to be negligible in accordance with the assumptions made in the Reynolds stresses closures.

The final form of the transport equations of $< u_i\theta >$ is

$$U_j\frac{\partial}{\partial x_j}(< u_i\theta >) = P_{i\theta} + D_{i\theta} + \phi_{i\theta} + \phi_{i\theta,w} \qquad (12)$$

$$P_{i\theta} = -\left(< u_iu_j > \frac{\partial T}{\partial x_j} + < u_j\theta > \frac{\partial U_i}{\partial x_j}\right)$$

$$D_{i\theta} = \frac{\partial}{\partial x_j}\left[(\alpha + \nu)\frac{\partial < u_i\theta >}{\partial x_j} + \frac{0.3k}{\varepsilon} < u_ju_l > \frac{\partial < u_i\theta >}{\partial x_l}\right]$$

$$\phi_{i\theta} = -C_{i\theta,1}\frac{\varepsilon}{k} < u_i\theta > +C_{i\theta,2} < u_l\theta > \frac{\partial U_i}{\partial x_l}$$

$$\phi_{i\theta,w} = \left[-0.1\frac{\varepsilon}{k} < u_i\theta > -0.02 < u_l\theta > \left(4\frac{\partial U_i}{\partial x_l} - \frac{\partial U_l}{\partial x_i}\right)\right]\frac{k^{\frac{3}{2}}}{\varepsilon x_n}$$

2.2.2 Scalar Triple Product Equations

In order to evaluate the triple products of velocity-temperature fluctuations, $< u_iu_j\theta >$, transport equations were formulated and are given as follows :

$$U_k\frac{\partial}{\partial x_k}(< u_iu_j\theta >) =$$

$$\underbrace{-\left(< u_iu_ju_k > \frac{\partial T}{\partial x_k} + < u_ju_k\theta > \frac{\partial U_i}{\partial x_k} + < u_ku_i\theta > \frac{\partial U_j}{\partial x_k}\right)}_{I}$$

$$\underbrace{-[< u_iu_j\frac{\partial}{\partial x_k}(u_k\theta - < u_k\theta >) > + < u_i\theta\frac{\partial}{\partial x_k}(u_ju_k - < u_ju_k >) >}_{II}$$

$$\underbrace{+ < u_j\theta\frac{\partial}{\partial x_k}(u_ku_i - < u_ku_i >) >]}_{II}$$

$$\underbrace{-\left(< u_iu_j\frac{\partial}{\partial x_k}(\alpha\frac{\partial\theta}{\partial x_k}) > + < u_i\theta\frac{\partial}{\partial x_k}(\frac{\mu}{\rho}\frac{\partial u_j}{\partial x_k}) > + < u_j\theta\frac{\partial}{\partial x_k}(\frac{\mu}{\rho}\frac{\partial u_i}{\partial x_k}) >\right)}_{III}$$

$$- \left(< \frac{u_i \theta}{\rho} \frac{\partial p}{\partial x_j} > + < \frac{u_j \theta}{\rho} \frac{\partial p}{\partial x_i} > \right) \qquad (13)$$

$$\underbrace{\phantom{- \left(< \frac{u_i \theta}{\rho} \frac{\partial p}{\partial x_j} > + < \frac{u_j \theta}{\rho} \frac{\partial p}{\partial x_i} > \right)}}_{IV}$$

which can be written as

$$U_k \frac{\partial}{\partial x_k} \left(< u_i u_j \theta > \right) = P_{ij\theta,1} + P_{ij\theta,2} + D_{ij\theta} + \phi_{ij\theta} - \varepsilon_{ij\theta} \qquad (14)$$

I   = Production rate due to the mean strain rate and temperature gradients

II   = Production rate due to the interactions of $< u_i u_j >$ and gradients of $< u_i u_j >$ with the heat flux components, $< u_i \theta >$

III   = Diffusive and dissipative effects due to molecular viscosity

IV   = Pressure-heat flux effects

In closing the above equations, term I needs no further modifications since it is explicit. Term II can be rearranged and written as:

$$II = < u_i u_j > \frac{\partial < u_k \theta >}{\partial x_k} + < u_i \theta > \frac{\partial < u_j u_k >}{\partial x_k} + < u_j \theta > \frac{\partial < u_k u_i >}{\partial x_k}$$
$$- \frac{\partial}{\partial x_k} \left(< u_i u_j u_k \theta > \right) \qquad (15)$$

The quadruple terms are assumed to be Gaussian and can be split up as

$$< u_i u_j u_k \theta > = < u_i u_j > < u_k \theta > + < u_j u_k > < u_i \theta > + < u_k u_i > < u_j \theta > \qquad (16)$$

Differentiating equation (16) with respect to x_k and substituting the result into equation (15) yields

$$II = - < u_j u_k > \frac{\partial < u_i \theta >}{\partial x_k} - < u_k u_i > \frac{\partial < u_j \theta >}{\partial x_k} - < u_k \theta > \frac{\partial < u_i u_j >}{\partial x_k} \qquad (17)$$

Term III can be rearranged and cast into the following form :

$$III = (\alpha + 2\nu) \frac{\partial}{\partial x_k} \left(\frac{\partial}{\partial x_k} < u_i u_j \theta > \right)$$
$$- \alpha \left(2 < \frac{\partial \theta}{\partial x_k} \frac{\partial u_i u_j}{\partial x_k} > + < \theta \frac{\partial^2 u_i u_j^*}{\partial x_k^2} > \right)$$
$$- \nu \left(2 < \frac{\partial u_i}{\partial x_k} \frac{\partial u_j \theta}{\partial x_k} > + < u_i \frac{\partial^2 u_j \theta^*}{\partial x_k^2} > \right)$$
$$- \nu \left(2 < \frac{\partial u_j}{\partial x_k} \frac{\partial u_i \theta}{\partial x_k} > + < u_j \frac{\partial^2 u_i \theta^*}{\partial x_k^2} > \right) \qquad (18)$$

The first term in equation (18) represents the laminar diffusion while the rest of the terms express the dissipative effects. Terms with asterisks (*) consist of second derivatives of the second moments and are assumed to be negligible. Empirical coefficients were optimized to compensate the effects of the asterisk terms. Term IV is the pressure-heat flux effects term, and can be modeled as [40]:

$$
\begin{aligned}
IV &\approx C_{t1} < u_i u_j \theta > \frac{\varepsilon}{k} + C_{t2} \left(< u_j u_k \theta > \frac{\partial U_i}{\partial x_k} + < u_k u_i \theta > \frac{\partial U_j}{\partial x_k} \right) \\
&= C_{\theta\gamma} < u_i u_j \theta > \frac{\varepsilon}{k}
\end{aligned}
\tag{19}
$$

where the second term in equation (19) is merged into term I of equation (13) and the coefficient $C_{\varepsilon\gamma}$ was adjusted accordingly.

The final form of the transport equations are given below as:

$$
U_k \frac{\partial}{\partial x_k} (< u_i u_j \theta >) = P_{ij\theta,1} + P_{ij\theta,2} + D_{ij\theta} + \phi_{ij\theta} - \varepsilon_{ij\theta}
\tag{20}
$$

where

$$
\begin{aligned}
P_{ij\theta,1} &= -\left[< u_i u_j u_k > \frac{\partial T}{\partial x_k} + < u_j u_k \theta > \frac{\partial U_i}{\partial x_k} + < u_k u_i \theta > \frac{\partial U_j}{\partial x_k} \right] \\
P_{ij\theta,2} &= -\left[< u_j u_k > \frac{\partial < u_i \theta >}{\partial x_k} + < u_k u_i > \frac{\partial < u_j \theta >}{\partial x_k} + < u_k \theta > \frac{\partial < u_i u_j >}{\partial x_k} \right] \\
D_{ij\theta} &= \frac{\partial}{\partial x_k} \left[(\alpha + 2\nu) \frac{\partial}{\partial x_k} < u_i u_j \theta > \right] \\
\phi_{ij\theta} &= -C_{\theta\gamma} \frac{\varepsilon}{k} < u_i u_j \theta > \\
\varepsilon_{ij\theta} &= C_{\theta\varepsilon} \frac{\varepsilon}{k} < u_k \theta > \frac{\partial \varepsilon}{\partial x_k}
\end{aligned}
$$

2.3 Pressure Strain Correlations

2.3.1 Formulation of a Pressure Strain Correlation

Following Chou [41], a Poisson equation for the fluctuating pressure, p, can be obtained by taking the divergence of the equation for the turbulent fluctuating velocity, u_i, which can be re-expressed to write the pressure-strain correlation as:

$$
< \frac{p}{\rho} \frac{\partial u_i}{\partial x_j} > = S_{ij} + \frac{1}{4\pi} \int_{vol} (T_{ij,1} + T_{ij,2}) \frac{d\,vol}{R}
\tag{21}
$$

where

$$T_{ij,1} = \left\langle \left(\frac{\partial^2 u_l u_m}{\partial x_l \partial x_m}\right)' \frac{\partial u_i}{\partial x_j} \right\rangle \tag{22}$$

$$T_{ij,2} = 2\left(\frac{\partial U_l}{\partial x_m}\right)' \left\langle \left(\frac{\partial u_m}{\partial x_l}\right)' \left(\frac{\partial u_i}{\partial x_j}\right) \right\rangle \tag{23}$$

$$R = |x - y| \tag{24}$$

where the first and second terms in the integral are denoted as $\phi_{ij,1}$ and $\phi_{ij,2}$, respectively, and S_{ij} is a surface integral which is negligible away from a solid wall. S_{ij} term is also developed and described in the next subsection.

Following Rotta's proposal [42], $\phi_{ij,1}$ was formulated same as one given by equation (5) with $C_{\phi_1} = 1.5$. Furthermore, $\phi_{ij,2}$ may be approximated as

$$\phi_{ij,2} = \frac{\partial U_l}{\partial x_m} \Pi_{lj}^{mi} \tag{25}$$

where Π_{lj}^{mi} is a fourth-order tensor which satisfies the kinematic constraints of

$$\Pi_{lj}^{mi} = \Pi_{lj}^{im} = \Pi_{jl}^{im} \tag{26}$$

$$\Pi_{li}^{mi} = 0 \tag{27}$$

$$\Pi_{jj}^{mi} = 2 < u_m u_i > \tag{28}$$

$$\Pi_{lj}^{ii} = 2 < u_l u_j > \tag{29}$$

Equation (25) suggests that Π_{lj}^{mi} can be approximated by a linear combination of the Reynolds stresses as:

$$
\begin{aligned}
\Pi_{lj}^{mi} = {} & A\frac{1}{k} < u_m u_i >< u_l u_j > + B\frac{1}{k} < u_m u_l >< u_i u_j > \\
& + C\frac{1}{k} < u_m u_j >< u_i u_l > + D\delta_{ij} < u_m u_i > \\
& + E(\delta_{ml} < u_i u_j > + \delta_{mj} < u_i u_l > \\
& + \delta_{il} < u_m u_j > + \delta_{ij} < u_m u_l >) \\
& + C_{\phi_2}\delta_{mi} < u_l u_j > + L\delta_{mi}\delta_{lj}k + M(\delta_{mj}\delta_{il} + \delta_{ml}\delta_{ij})k
\end{aligned} \tag{30}
$$

where the condition of equation (26) is already imposed. The application of equations (27) through (29) enables two of these constants to be expressed in terms of the third, namely C_{ϕ_2} and can be written as

$$
\begin{aligned}
A &= B = -C = \left(\frac{10 - 7C_{\phi 2}}{2}\right) \\
D &= C_{\phi_2} \\
E &= C_{\phi_2} - 2 \\
L &= -\left(\frac{4 + 2C_{\phi_2}}{5}\right) \\
M &= \left(\frac{6 - 2C_{\phi_2}}{5}\right)
\end{aligned}
$$

The final form is given as

$$
\begin{aligned}
< \frac{p}{\rho}\left(\frac{\partial u_i}{\partial x_j} + \frac{\partial u_j}{\partial x_i}\right) > &= -C_{\phi_1}\frac{\epsilon}{k}\left(< u_i u_j > -\frac{2}{3}\delta_{ij}k\right) \\
&+ (7C_{\phi_2} - 10)G\left(\frac{< u_i u_j >}{k} - \frac{2}{3}\delta_{ij}\right) \\
&- 2(C_{\phi_2} - 1)(G_{ij} - \frac{2}{3}\delta_{ij}G) \\
&- 2(C_{\phi_2} - 1)(H_{ij} - \frac{2}{3}\delta_{ij}G) \\
&- \frac{2}{5}(2C_{\phi_2} - 1)\left(\frac{\partial U_i}{\partial x_j} + \frac{\partial U_j}{\partial x_i}\right)k
\end{aligned} \tag{31}
$$

The coefficient C_{ϕ_2} can be determined by simplifying the Reynolds stresses described by equation (1) into an algebraic equation which was originally developed by Rodi [43].

If the convection-diffusion string of the $< u_i u_j >$ is set equal to that of the turbulence kinetic energy, k, it follows that,

$$
\frac{\partial}{\partial x_l}(U_l < u_i u_j >) - D_{ij} = \frac{< u_i u_j >}{k}\left[\frac{\partial}{\partial x_l}(U_l k) - D_k\right] \tag{32}
$$

where D_{ij} and D_k denote, respectively, the diffusion rates of $< u_i u_j >$ and k. After some manipulation, equation (32) can be re-arranged into the following form,

$$
\begin{aligned}
\frac{< u_i u_j >}{k} - \frac{2}{3}\delta_{ij} &= -\left[\frac{(2C_{\phi_2} - 3)(G_{ij} - \frac{2}{3}\delta_{ij}G) + (2C_{\phi_2} - 2)(H_{ij} - \frac{2}{3}\delta_{ij}G)}{C_{\phi_1}\epsilon + 10G - 7C_{\phi_2}G}\right] \\
&- \left(\frac{4C_{\phi_2} - 2}{C_{\phi_1}\epsilon + 10G - 7C_{\phi_2}G}\right)\frac{k}{5}\left(\frac{\partial U_i}{\partial x_j} + \frac{\partial U_j}{\partial x_i}\right)
\end{aligned} \tag{33}
$$

By assuming that the dissipative action is isotropic, and the flow is parabolic, equation (33) can be further reduced to :

$$\frac{<uu>}{k} - \frac{2}{3} = -\frac{(4C_{\phi_2} - 8)}{3(C_{\phi_1} - 7C_{\phi_2} + 10)} = 0.3 \qquad (34)$$

$$\frac{<vv>}{k} - \frac{2}{3} = -\frac{(4C_{\phi_2} - 2)}{3(C_{\phi_1} - 7C_{\phi_2} + 10)} = -0.18 \qquad (35)$$

$$\frac{<ww>}{k} - \frac{2}{3} = -\frac{(10 - 8C_{\phi_2})}{3(C_{\phi_1} - 7C_{\phi_2} + 10)} = -0.12 \qquad (36)$$

The above set of relations are compared with typical experimental data for several parabolic flows, and the coefficient C_{ϕ_2} is found as:

$$C_{\phi_2} = 1.05$$

2.3.2   Formulation of a Near Wall Model

In parallel to the former derivation for the pressure-strain correlation the near-wall correlation can be set as:

$$(\phi_{ij,w} + \phi_{ji,w}) = \left[C'_{\phi_1} \frac{\epsilon}{k} (< u_i u_j > -\frac{2}{3}\delta_{ij}k) + \frac{\partial U_l}{\partial x_m}(\Omega_{lj}^{mi} + \Omega_{li}^{mj}) \right] f\left(\frac{l}{y}\right) \qquad (37)$$

where the function $f(l/y)$ represents the wall controlling function which enforces the total term become negligible in the region away from a solid wall. If the forth-order tensor Ω_{lj}^{mi} is expanded, we have

$$
\begin{aligned}
\Omega_{lj}^{mi} = &\ A'\frac{1}{k} < u_m u_i >< u_l u_j > + B'\frac{1}{k} < u_m u_l >< u_i u_j > \\
&+ \ C'\frac{1}{k} < u_m u_j >< u_i u_l > + D'\delta_{ij} < u_m u_i > \\
&+ \ E'(\delta_{ml} < u_i u_j > + \delta_{mj} < u_i u_l > \\
&+ \ \delta_{il} < u_m u_j > + \delta_{ij} < u_m u_l >) \\
&+ \ C'_{\phi_2}\delta_{mi} < u_l u_j > + L'\delta_{mi}\delta_{lj}k + M'(\delta_{mj}\delta_{il} + \delta_{ml}\delta_{ij})k \qquad (38)
\end{aligned}
$$

where the following conditions are imposed.

$$\Omega_{li}^{mi} = 0 \tag{39}$$

$$\frac{<uu>}{k} - \frac{2}{3} = 0.51 \tag{40}$$

$$\frac{<vv>}{k} - \frac{2}{3} = -0.42 \tag{41}$$

$$\frac{<ww>}{k} - \frac{2}{3} = -0.09 \tag{42}$$

$$-\frac{<uv>}{k} = 0.24 \tag{43}$$

In equations (39) through (43), these experimental data are introduced from Champagne et al. [44] in order to solve the coefficients in terms of C_{ϕ_2}.

Experimental data of Champagne et al. [44] were used to obtain the coefficients in equations (39) through (43) in terms of C_{ϕ_2}.

$$
\begin{aligned}
A' &= -C' \\
B' &= 0 \\
E' &= 0.11C_{\phi_2} \\
D' &= -1.70C_{\phi_2} \\
L' &= M' = -0.04C_{\phi_2}
\end{aligned}
$$

Then the final form of the second term in the parentheses of equation (21) becomes:

$$
\begin{aligned}
\frac{\partial U_l}{\partial x_m}(\Omega_{lj}^{mi} + \Omega_{li}^{mj}) &= 1.55C_{\phi_2}G_{ij} - 0.21C_{\phi_2}G - 0.11C_{\phi2}H_{ij} \\
&\quad - C'_{\phi_2}H_{ij} - 0.08C_{\phi_2}\left(\frac{\partial U_i}{\partial x_j} + \frac{\partial U_j}{\partial x_i}\right)k
\end{aligned} \tag{44}
$$

As before if equation (27) is substituted into the algebraic stresss equation (equation (32)) then, after considerable manipulation. We obtain as:

$$\frac{<uu>}{k} - \frac{2}{3} = \frac{(2.67 + 1.56C_{\phi_2})}{(C_{\phi_1} - 7C_{\phi_2} + 10 - C'_{\phi_1})} = 0.51 \tag{45}$$

$$\frac{<vv>}{k} - \frac{2}{3} = \frac{(0.67 - 1.76C_{\phi_2} - 2C'_{\phi_2})}{(C_{\phi_1} - 7C_{\phi_2} + 10 - C'_{\phi_1})} = -0.42 \tag{46}$$

$$\frac{<ww>}{k} - \frac{2}{3} = \frac{(2.45C_{\phi_2} - 3.33)}{(C_{\phi_1} - 7C_{\phi_2} + 10 - C'_{\phi_1})} = -0.09 \tag{47}$$

$$-\frac{<uv>}{k} = \left[\frac{0.88C_{\phi_2} - 0.4}{C_{\phi_1} - 7C_{\phi_2} + 10 - C'_{\phi_1}}\right]^{0.5} \bullet$$
$$\left[\frac{(3 - 0.45C_{\phi_2})\frac{<vv>}{k} - (C'_{\phi_2} - 2 + 2.11C_{\phi_2})\frac{<uu>}{k}}{C_{\phi_1} - 7C_{\phi_2} + 10 - C'_{\phi_1}}\right]^{0.5} \tag{48}$$

As before by comparing with the experimental data of Champagne et al., coefficients are obtained as follow:

$$C'_{\phi_1} = -4.28 \tag{49}$$

$$C'_{\phi_2} = 1.18 \tag{50}$$

2.4 Constants Used in the Computations

Hydrodynamics Equations

Table 1 lists the values of all constants used in the hydrodynamics equations.

Heat Transfer Equations

Table 2 lists the numerical values of constants used in heat transfer equations.

Variable	Numerical values
C_ϵ	0.30
C_{ϕ_1}	1.5
C_{ϕ_2}	0.4 $\star$
C_ν	0.09
C_γ	3.0 †
$C_{\gamma w}$	8.0
$C_{\epsilon\gamma}$	0.30
C_1	1.44
C_2	1.92
C_{11}	1.21
C_{12}	-0.24
C_{22}	0.24
C_l	2.55
C_s	0.25
α_1	-8.14×10^{-3}
α_2	-1.72×10^{-2}
α_3	-4.80×10^{-2}
α_4	-1.02×10^{-1}
κ	0.42
σ_k	1.0

$\star$ The values of C_{ϕ_2} for parabolic code are:
= 0.75 for model of Amano et al
= 0.6 for model of Naot et al
† The value of C_γ for high-Reynolds number model = 5.8

Table 1: Values of Hydrodynamics constants.

Variable	Numerical values
C_{1T}	0.31
C_{2T}	0.16
$C_{\theta\gamma}$	6.0
$C_{\theta\epsilon}$	0.10
$C_{i\theta,1}$	3.2
$C_{i\theta,2}$	0.5

Table 2: Values of heat transfer constants.

2.5 Boundary Conditions

The numerical solutions of the transport equations require the provision of good boundary values and this section describes the treatments of boundary nodes used in this study.

2.5.1 Backward-Facing Step Flow

Inlet Conditions

The U-velocity is calculated from the step-height Reynolds number and assumed to be uniform throughout the inlet section of the computation domain. V-velocity is set to zero.

The turbulent kinetic energy and turbulent energy dissipations are computed from the inlet turbulent intensities by the following relations:

$$k = iU_{IN}^2 \tag{51}$$

$$\varepsilon = \frac{k^{\frac{3}{2}}}{\lambda H} \tag{52}$$

The inlet Reynolds stresses are given the following values:

$$< uu > = \frac{2}{3}k \tag{53}$$

$$< vv > = \frac{2}{3}k \tag{54}$$

$$< uv > = -0.01k \tag{55}$$

The inlet values of the third moments velocity products are specified by the algebraic model of Daly and Harlow [45] as

$$< u_i u_j u_k > = -0.25\frac{k}{\varepsilon} < u_k u_l > \frac{\partial < u_i u_j >}{\partial x_l} \tag{56}$$

The inlet temperature is set to the value used in the experiment. While the second-moment of velocity-temperature products are specified by assuming that fluctuating quantities are 5% of the mean quantities. This can be written as:

$$< u_i \theta > = (0.05)^2 T_{IN} U_{IN} \tag{57}$$

The triple products of velocity-temperature correlations are specified by using model of Launder [39] as:

$$< u_i u_j \theta > = -0.10 \frac{2k}{\varepsilon} \left(< u_i u_l > \frac{\partial < u_j \theta >}{\partial x_l} + < u_j u_l > \frac{\partial < u_i \theta >}{\partial x_l} \right) \qquad (58)$$

Initial Values

The initial values for U-velocities are set by using the conservation of mass, which reduces to $U_{IN} Y_0 = U D_c$ for incompressible flows. The V velocities are given zero values.

The turbulent kinetic energy, turbulent energy dissipation and Reynolds stresses are given constant values of equal magnitudes with the respective inlet conditions.

The initial values of triple products of velocity are prescribed by the algebraic equation of Daly and Harlow [45].

All initial values of heat transfer variables are the same as their respective inlet values.

Wall Boundary Conditions

At the wall boundary, the wall function treatments are employed for the momentum and the turbulent kinetic energy. For the mean momentum equations, the velocity gradient is used to determine the wall shear stress which is then used to prescribe the boundary values. For the turbulent kinetic energy, the wall shear stress is incorporated into the generation rate and thus introducing the wall effects.

The dissipation rate is evaluated under the local equilibrium condition in terms of the turbulent kinetic energy as

$$\varepsilon = \frac{k^{\frac{3}{2}}}{C_l x_n} \qquad (59)$$

Launder et al. [36] obtained a correlation between $< u_i u_j >$ and U_τ for channel flows as

$$< u_i u_j > = C_{ij} U_\tau^2 - (1. - \delta_{ij}) \frac{y_1}{\rho} \frac{dP}{dy_2} \qquad (60)$$

The coefficients C_{ij} are given as

$$C_{11} = 5.1$$
$$C_{12} = -1.0$$
$$C_{22} = 1.0$$

Using the correlation of k and U_τ in the wall proximity derived by Hanjalic and Launder [24]:

$$k \approx 3.5 U_\tau^2 \tag{61}$$

the boundary values of $< u_i u_j >$ can be expressed in terms of k as:

$$< u_i u_j >= C_{ij} k - (1. - \delta_{ij}) \frac{y_1}{\rho} \frac{dP}{dy_2} \tag{62}$$

where the coefficients C_{ij} are now

$$C_{11} = 1.214$$
$$C_{12} = -0.24$$
$$C_{22} = 0.24$$

The algebraic equation of Shir [46] was combined with the wall values of $< u_i u_j >$ to prescribe the wall values of $< u_i u_j u_k >$ and is given as follow:

$$< u_i u_j u_k >= 0.04 \frac{k^2}{\varepsilon} \frac{\partial}{\partial x_k} \left[C_{ij} k - (1. - \delta_{ij}) \frac{y_1}{\rho} \frac{dP}{dy_2} \right] \tag{63}$$

For the temperature equation, a constant heat flux of 270 w/m is applied along the wall downstream of the step. The heat flux is introduced into the solution domain by supplementing the source term at the wall adjacent cell for the temperature equation with this heat flux.

The wall boundary conditions for $< u_i \theta >$ are based on the fact that at the wall,

$$< u\theta >=< v\theta >= 0.0$$

Therefore, the value of $< v\theta >$ at the wall adjacent node is set by interpolation between the wall and the node next to the wall adjacent node. The value of $< u\theta >$ at the wall adjacent node is set equal to minus twice the value of $< v\theta >$ [39].

Since the velocity-temperature products $< u_i u_j \theta >$ fall to zero at the wall, the near-wall values, hence, were made very small such that zero wall values is obtained.

Outflow Conditions

Zero streamwise gradient conditions are used as the outflow conditions for all variables with the exception of the U momentum and temperature.

The law of conservation of mass is used as the outflow condition for U momentum.

The outflow temperature distribution is prescribed in accordance with Kays and Crawford [47] as

$$\frac{dT}{dx} = \frac{2\dot{q}_w''}{\rho C_P U D_c}$$

2.5.2 Turbulent Jet Flow

Inlet Conditions

In the self-preserved region of the jets, the U-velocity is assumed to follow the cosine curve. Therefore, a cosine function is used to describe the inlet U-velocity with the amplitude of the free stream velocity. V-velocity is assumed to be zero at the nozzle.

The turbulent kinetic energy and turbulent energy dissipation is prescribed by the following relations:

$$k = C_\mu^{-\frac{1}{2}} l_m^2 \left(\frac{\partial U}{\partial y}\right)^2 \tag{64}$$

$$\varepsilon = C_\mu^{\frac{1}{2}} k \frac{\partial U}{\partial y} \tag{65}$$

where l_m is the minimum of the wall mixing length and the Nikuradse's formula. Both formulae are listed below with the wall mixing length relation first, and followed by Nikuradse' formula.

$$l_m = 0.41y \tag{66}$$

$$\frac{l_m}{r_N} = 0.14 - 0.08\left(1 - \frac{y}{r_N}\right)^2 - 0.06\left(1 - \frac{y}{r_N}\right)^4 \tag{67}$$

The Reynolds stresses are prescribed by using the Boussinesq viscosity correlations as

$$-\rho < u_i u_j > = \mu_t \left(\frac{\partial U_i}{\partial x_j} + \frac{\partial U_j}{\partial x_i}\right) - \frac{2}{3}\delta_{ij}k \tag{68}$$

The inlet temperature is given the value described in the experiment.

Chapter 3

Numerical Procedure

3.1   Elliptic Code

3.1.1   Discretization of Governing Equations

The steady state, two dimensional governing equations of all dependent variables solved in the backward-facing step flows can be written in the following form

$$\frac{\partial}{\partial x}(\rho U \phi) + \frac{\partial}{\partial y}(\rho V \phi) = \frac{\partial}{\partial x}\left[\Gamma_1 \frac{\partial \phi}{\partial x}\right] + \frac{\partial}{\partial y}\left[\Gamma_2 \frac{\partial \phi}{\partial y}\right] + S_\phi \tag{69}$$

where ϕ is the dependent variable $U, V, k, \varepsilon, < u_i u_j >, \ldots$. This equation is divided into three general parts, namely convection of ϕ, diffusion of ϕ and source term of ϕ
.

Equation (69) is discretized to a linear algebraic equation before solution of dependent variables can be obtained. Before proceeding further, a few definitions of grid system must be made. Figure 2 outlines detail definitions of geometrical dimensions and locations. Letters P,E,W,N,S are the node P inside it's control volume and it's neighboring nodes East, West, North, and South, respectively. The letters e,w,n,s are the control surfaces of P control volume at east,west,north and south, respectively.

Discretization of equation (69) is carried out by using the control volume approach of Patankar [48, 49]. The final form of the discretization equation using central differencing scheme is as follow:
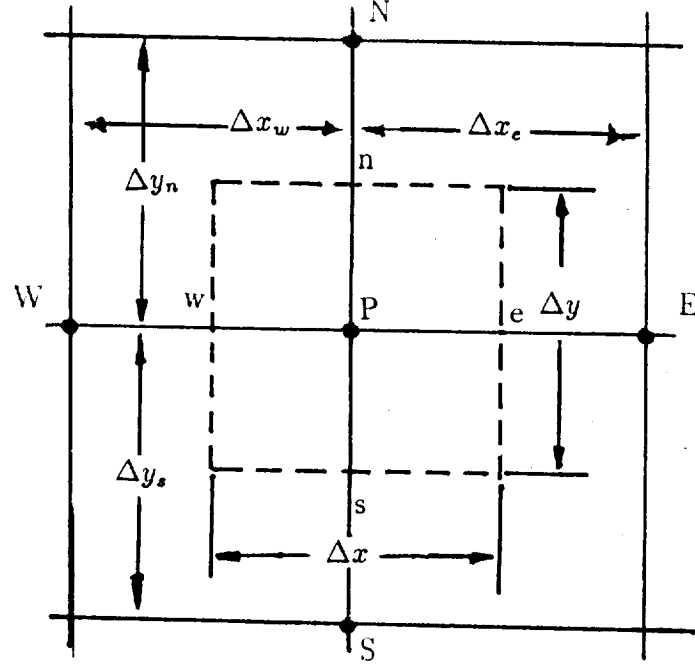
Figure 2: Definitions of geometrical dimensions and locations.

$$a_P \phi_P = a_E \phi_E + a_W \phi_W + a_N \phi_N + a_S \phi_S + b \tag{70}$$

where

$$a_N = \frac{\Gamma_{2n}}{\Delta y_n} \Delta x - \frac{1}{2} \rho V_n \Delta x$$

$$a_S = \frac{\Gamma_{2s}}{\Delta y_s} \Delta x - \frac{1}{2} \rho V_s \Delta x$$

$$a_E = \frac{\Gamma_{2e}}{\Delta x_e} \Delta y - \frac{1}{2} \rho U_e \Delta y$$

$$a_W = \frac{\Gamma_{2w}}{\Delta x_w} \Delta y - \frac{1}{2} \rho U_w \Delta y$$

$$a_P = a_E + a_W + a_N + a_S - S_P \Delta x \Delta y$$

$$b = S_U \Delta x \Delta y$$

Although central differencing scheme has second order accuracy, it is not used in the computations because some of the coefficients, a_i might be negative at certain iterations. This is violating the four basic rules which can result in physically unrealistic solutions. As a result, a new scheme called upwind differencing scheme

scheme	Formula for A($\mid P \mid$)
Central Difference	$1 - 0.5 \mid P \mid$
Upwind	1
Hybrid	$\parallel 0, 1 - 0.5 \mid P \mid \parallel$
Power law	$\parallel 0, (1 - 0.5 \mid P \mid)^5 \parallel$
Exponential	$\mid P \mid /(\exp \mid P \mid - 1)$

Table 3: A($\mid P \mid$) for various differencing schemes.

was introduced. This scheme has a set back because it only has first order accuracy. Spalding [50] proposed a scheme that combines the advantages of central differencing and upwind differencing schemes and called it hybrid differencing scheme. With minor modifications, the general discretization equation can be written as:

$$a_P \phi_P = a_E \phi_E + a_W \phi_W + a_N \phi_N + a_S \phi_S + b \tag{71}$$

where

$$
\begin{aligned}
a_N &= D_n A(|P_n|) + \parallel -F_n, 0 \parallel \\
a_S &= D_s A(|P_s|) + \parallel F_s, 0 \parallel \\
a_E &= D_e A(|P_e|) + \parallel -F_e, 0 \parallel \\
a_W &= D_w A(|P_w|) + \parallel F_w, 0 \parallel \\
a_P &= a_E + a_W + a_N + a_S - S_P \Delta x \Delta y \\
b &= S_U \Delta x \Delta y
\end{aligned}
$$

and

$$D_e = \frac{\Gamma_{1e}}{\Delta x_e}\Delta y, \quad D_w = \frac{\Gamma_{1w}}{\Delta x_w}\Delta y, \quad D_n = \frac{\Gamma_{2n}}{\Delta y_n}\Delta x, \quad D_s = \frac{\Gamma_{2s}}{\Delta y_s}\Delta x$$

$$P_e = \frac{(\rho U)_e}{D_e}\Delta y, \quad P_w = \frac{(\rho U)_w}{D_w}\Delta y, \quad P_n = \frac{(\rho V)_n}{D_n}\Delta x, \quad P_s = \frac{(\rho V)_s}{D_s}\Delta x$$

$$F_e = (\rho U)_e \Delta y, \quad F_w = (\rho U)_w \Delta y, \quad F_n = (\rho V)_n \Delta x, \quad F_s = (\rho V)_s \Delta x \tag{72}$$

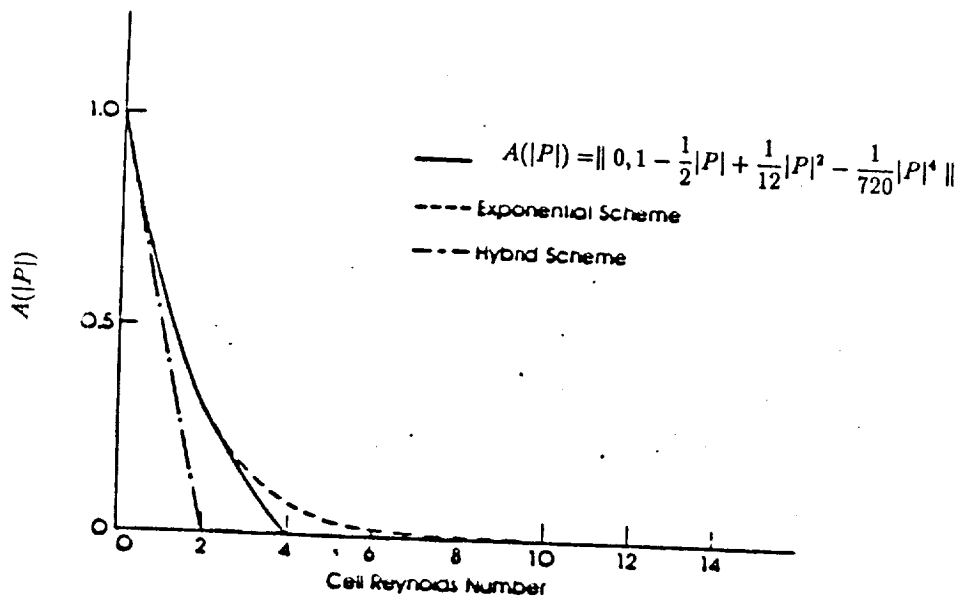the formulae for $A(|P|)$ are listed in table 3 for various schemes.

Figure 3: Function A(| P |) for three different schemes.

Since the goodness of different schemes are based on profile fitting with the one dimensional analytic solution, Amano [51] proposed a fourth order differencing scheme by expanding the exponential scheme of Spalding and found that this scheme gives better agreement with the exponential scheme than the hybrid scheme. Figure 3 shows the graph of $A(|P|)$ and the fourth order scheme is indeed better than the hybrid scheme. The formula of $A(|P|)$ for the fourth order scheme can be written as:

$$A(|P|) = \| \, 0, 1 - \frac{1}{2}|P| + \frac{1}{12}|P|^2 - \frac{1}{720}|P|^4 \, \|$$

(73)

3.1.2 Grid System

The grid system used in this study is the so-called staggered grid system in which all scalar quantities are associated with every grid node (i.e. points where grid lines intersect), while the U-cell is displaced half a node leftward, V-cell half a node downward and $< uv >$-cell both half a node leftward and downward. Figure 4 shows the grid, storage locations and control volumes of all dependent variables. The grid system is advantageous in solving the velocity field because the pressure gradients
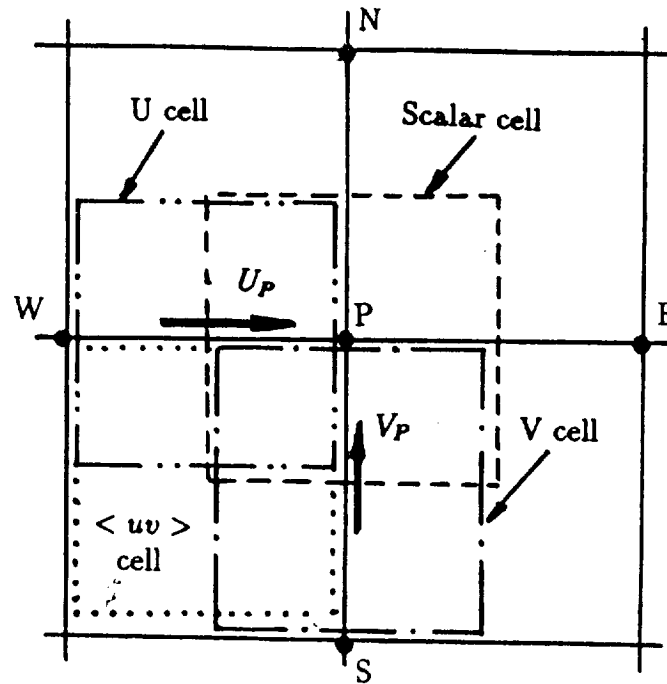
Figure 4: Staggered grid system and the grid storage locations used in elliptic computations.

can be evaluated easily and velocities are conveniently located for the evaluation of convective fluxes [20].

3.1.3 Solution of Discretization Equation

After the formulation of the discretization equation, a line by line iterative method is used to obtain solutions for all dependent variables. The solution domain is given some initially guessed values which are improved upon from one line to the other. In this procedure, the values of ϕ on neighboring lines are assumed to be temporarily known. This, then reduces the unknowns to be solve to three and turns the discretization equation into a convenient algorithm sometimes called the Thomas algorithm or the TDMA (Tri-Diagonal-Matrix Algorithm). This algorithm is used along the North-South line and swept from west to east of the solution domain. A more detail explanation of the algorithm is given by Amano [52].

3.1.4 Pressure and Velocity Corrections

At this stage, all dependent variables can be evaluated by the TDMA algorithm except the pressure field. The pressure gradient forms part of the source term in the momentum equations. If the correct pressure distributions of the solution domain are known, there will be no difficulty in the solution of the momentum equations.

As mentioned before, the solution domain was given some guess values which most likely were not the correct distributions for most variables. This made the solution of the momentum equations impossible (due to incorrect pressure field). To correct this problem, the pressure field is indirectly specified via the continuity equation. When the correct pressure field is substituted into the momentum equations, the resulting velocities fields satisfies the continuity equation also.

This indirect substitution of the pressure field is called the SIMPLE algorithm (Semi-Implicit Method for Pressure-Linked Equation). Patankar [48, 49] outlined the SIMPLE algorithm in its detail.

3.2 Parabolic Code

3.2.1 Discretization of Governing Equations

The steady state, two-dimensional parabolic flows governing equations can be written in the general form of:

$$\frac{\partial}{\partial x}(\rho U \phi) + \frac{\partial}{\partial y}(\rho V \phi) = \frac{\partial}{\partial y}\left[\Gamma \frac{\partial \phi}{\partial y}\right] + S_\phi \tag{74}$$

where ϕ is again the dependent variable $U, V, k, \varepsilon, < u_i u_j > \dots$ The only difference between equation (74) and equation (69) is the omission of axial diffusion in parabolic flows.

Equation (74) is discretized to a linear algebraic equation following Patankar's finite-volume approach with hybrid differencing scheme for advection and central differencing scheme for diffusion terms, respectively.

The final form of the discretization equation using hybrid differencing is as follow

$$a_P \phi_P = a_E \phi_E + a_W \phi_W + a_N \phi_N + a_S \phi_S + b \tag{75}$$

where

$$a_N = D_n A(|P_n|) + \parallel -F_n, 0 \parallel$$
$$a_S = D_s A(|P_s|) + \parallel F_s, 0 \parallel$$
$$a_E = 0.0$$
$$a_W = \parallel F_w, 0 \parallel$$
$$a_P = a_E + a_W + a_N + a_S - S_P \Delta x \Delta y$$
$$b = S_U \Delta x \Delta y$$

The definitions of all variables are given in equation (72) and $A(|P|)$ is the hybrid differencing scheme given in table 3. The coefficient a_E is set to zero because there are no influence from downstream nodes for parabolic flows.

3.2.2 Grid System

In this code, the grid system used is slightly different from the one used in elliptical computations. In this system, all scalar quantities including the Reynolds shear stress, $< uv >$, are associated with the grid node, while U-cell and V-cell are displaced half a node leftward and downward respectively. Figure 5 shows the grid storage locations and control volumes of all dependent variables.

3.2.3 Solution of Discretization Equation

After formulating the discretization equation, a line by line noniterative procedure is used to obtain solution for all dependent variables based on the known upstream values. A noniterative procedure is used as compared to the iterative procedure in elliptic computations because there are no downstream influence in parabolic flows.

3.3 Boundary Conditions

In this study, the grids are arranged such that cell boundaries coincide with edges of the solution domain. Figure 6 depicts a typical grid and solution domain arrangement. Since some nodes lie outside of the solution domain, the solution is not influenced by these nodes. As a result, the coefficients for these nodes must be
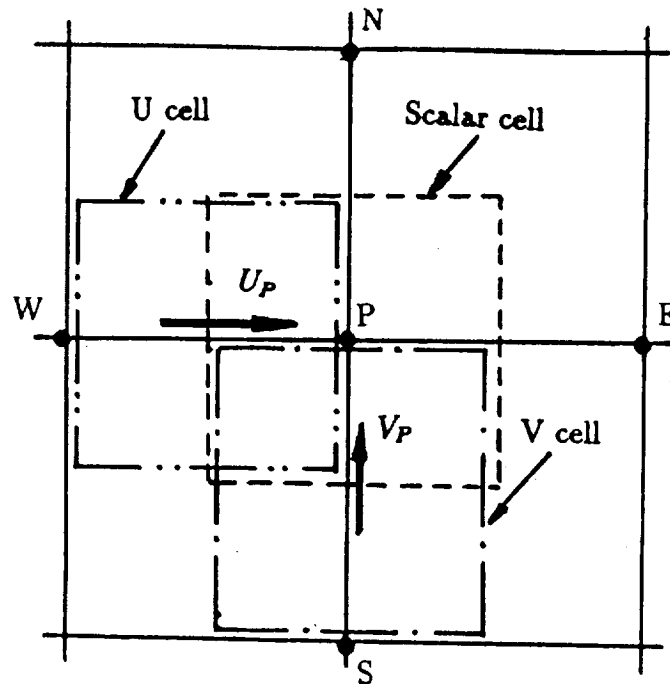
Figure 5: Grid storage locations and control volumes used in parabolic computations.

set to zero. In figure 7, point W lies outside of the solution domain. Therefore, at point P, the coefficient a_W must be set to zero. At this point, the correct value may be added through the source term. Generally, there are three types of boundary conditions, these are the Dirichlet condition (Prescribed values of ϕ_B), Neumann condition (prescribed flux at boundary) and Robin condition (boundary flux specified via a coefficient and condition of surrounding fluid). Apart from these, there is a so-called internal condition, where any internal node can be set to a desired value of ϕ_P. Amano [52, 53] outlined the mathematical formulations for the treatments of these conditions.

3.4   Grid Generation

An algebraic grid generation technique was developed to generate boundary conforming grids for two-dimensional duct flows. In this technique the grid point locations on the top and bottom boundaries are given, and the grid points in the interior of the domain are computed along straight lines connecting the corresponding top and bottom boundary grid points. The method described here allows for the
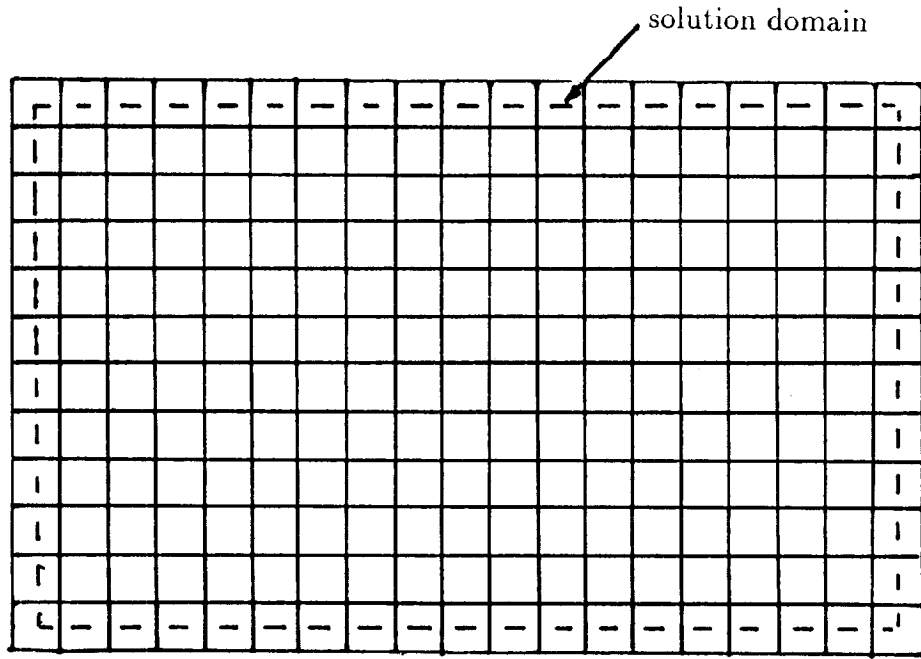
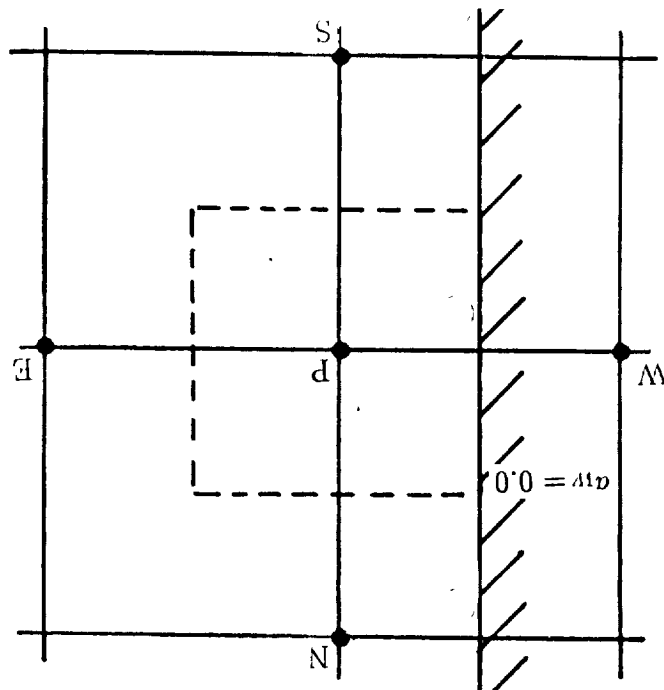Figure 6: Typical grid and solution domain.

Figure 7: Boundary node.

generation of grids with the grid line spacing next to the walls kept at a constant user specified value.

If $(N - 2)$ grid points are to be distributed along a straight line between the grid points (x_1, y_1) and (x_N, y_N), and if the spacing between the points (x_1, y_1) and (x_2, y_2) and the spacing between the points (x_{N-1}, y_{N-1}) and (x_N, y_N) is to be a user specified value, $(\Delta s)_1$, then the expansion factors in the x and y directions are given as:

$$\beta_x = \left[1 + \frac{\Delta X (\beta_x - 1)}{2(\Delta x)_1} \right]^{\frac{2}{N-1}} \tag{76}$$

$$\beta_y = \left[1 + \frac{\Delta Y (\beta_y - 1)}{2(\Delta y)_1} \right]^{\frac{2}{N-1}} \tag{77}$$

where

$$\Delta X = x_N - x_1 \tag{78}$$

$$\Delta Y = y_N - y_1 \tag{79}$$

$$(\Delta y)_1 = sign(\Delta Y) \frac{(\Delta s)_1}{\sqrt{1 + \left(\frac{\Delta X}{\Delta Y} \right)^2}} \tag{80}$$

$$(\Delta x)_1 = (\Delta y)_1 \frac{\Delta X}{\Delta Y} \tag{81}$$

Since the equations for the expansion factors β_x and β_y cannot be solved explicitly, it is necessary to iterate. Fixed point iteration using the expressions in the form shown above was found to converge within a few iterations, and was used to generate all the grids shown here. Once the expansion factors are known, the grid point locations are given by:

$$x_n = x_1 + (\Delta x)_1 \frac{(\beta_x)^{n-1} - 1}{\beta_x - 1} \qquad for \ n \leq \frac{N+1}{2} \tag{82}$$

$$y_n = x_1 + (\Delta y)_1 \frac{(\beta_y)^{n-1} - 1}{\beta_y - 1} \qquad for \ n \leq \frac{N+1}{2} \tag{83}$$

$$x_n = x_N - (\Delta x)_1 \frac{(\beta_x)^{N-n} - 1}{\beta_x - 1} \qquad for \ n > \frac{N+1}{2} \qquad (84)$$

$$y_n = y_N - (\Delta y)_1 \frac{(\beta_y)^{N-n} - 1}{\beta_y - 1} \qquad for \ n > \frac{N+1}{2} \qquad (85)$$

The method shown here was found to be very efficient, and could be used for many different geometries.

3.5 Coordinate Transformation

Equations (69) are transformed from the Cartesian coordinates (x, y) into generalized curvilinear coordinates (ξ, η). Consider the general steady state two-dimensional transport equation in the following form:

$$(\rho U \phi)_x + (\rho V \phi)_y = (\Gamma \phi_x)_x + (\Gamma \phi_y)_y + R_\phi(x, y) \qquad (86)$$

where Γ represents a diffusion coefficient and R_ϕ shows a source term of the transport equation of a dependent variable ϕ. Equation (86) can be written as

$$\frac{1}{J}[(\rho \tilde{U} \phi)_\xi + (\rho \tilde{V} \phi)_\eta] = \frac{1}{J}\left[\frac{\Gamma}{J}(\alpha \phi_\xi - \beta \phi_\eta)\right]_\xi + \frac{1}{J}\left[\frac{\Gamma}{J}(\gamma \phi_\eta - \beta \phi_\xi)\right]_\eta + S_\phi(\xi, \eta) \qquad (87)$$

where $S_\phi(\xi, \eta)$ is the transformed version of the source term $R_\phi(x, y)$ and where

$$J = x_\xi y_\eta - x_\eta y_\xi \qquad (88)$$

$$\alpha = x_\eta^2 + y_\eta^2 \qquad (89)$$

$$\beta = x_\xi x_\eta + y_\xi y_\eta \qquad (90)$$

$$\gamma = x_\xi^2 + y_\xi^2 \qquad (91)$$

In Eq.(87) the contravariant velocities $\tilde{U}$ and $\tilde{V}$ are given as:

$$\tilde{U} = U y_\eta - V x_\eta \qquad (92)$$

$$\tilde{V} = V x_\xi - U y_\xi \qquad (93)$$

Equation (87) is discretized by using the control volume method described in the following section.

3.5.1 Numerical Procedure for Transformed Coordinate System

Formulation and discretization of all transport equations were performed by using the conventional control-volume approach of Patankar [48],by breaking each equation into diffusion, convection, and source terms. The system of equations were made linear so that they could be solved iteratively by the tridiagonal matrix algorithm. After several numerical tests, it was observed that the variation in results of mean velocity profiles lies within 2% when the grid is changed from 52 x 52 to 62 x 62 for the computations of an angles backward facing step flow (Figure 8). Therefore the grid independent state was assumed to be attained with the grid of 62 x 62.

3.5.2 Pressure Correction Algorithm

Three pressure correction algorithm were tested: SIMPLE [55], SIMPLEC [56], and PISO [57]. Here we review the approximations made by the three algorithms.

SIMPLE

The SIMPLE (Semi-Implicit Method for Pressure Linked Equations) algorithm can be derived by first obtaining a discretized form of a velocity correction equation. The U-component velocity correction equations:

$$A_p U_p' = \Sigma A_{nb} U_{nb}' - y_\eta P_\xi' + y_\xi P_\eta' \tag{94}$$

where A's are the influence coefficients, and U' and P' are the velocity and pressure corrections. A with the subscript nb denotes the neighbor coefficients. If the above equation were used in the derivation of the pressure correction equation, an unmanageable equation would result. Instead, it is assumed that the velocity correction at a point is not affected by the velocity corrections of its neighbors, and thus the summation term in equation (94) is neglected.

SIMPLEC

The SIMPLEC (SIMPLE Consistent) algorithm attempt to use a more consistent approximation, based on the magnitude of the terms in the velocity correction equation. Instead of neglecting the velocity corrections at the neighboring points, the term
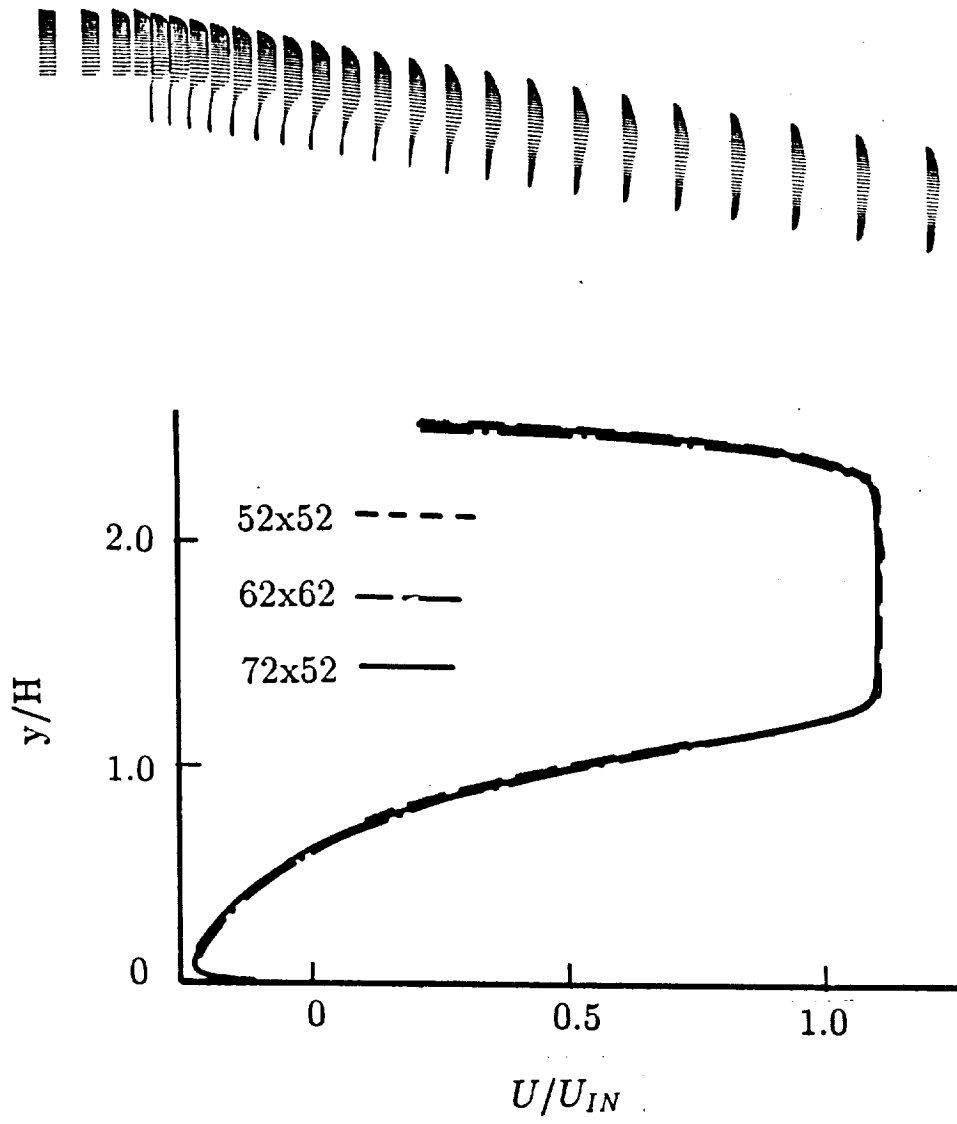
Figure 8: Velocity vectors and grid test for a backward facing step with 10° bent.

$\Sigma A_{nb}U'_p$ is subtracted from both sides of equation (94). This leads to the following:

$$(A_p - \Sigma A_{nb})U'_p = \Sigma A_{nb}(U'_{nb} - U'_p) - y_\eta P'_\xi + y_\xi P'_\eta \qquad (95)$$

Again, if the above equation were used to form the pressure correction equation, an unmanageable equation would result. In the SIMPLEC algorithm the summation term on the right hand side is neglected.

PISO

In the PISO (Pressure Implicit with Splitting of Operators) algorithm the pressure and velocities are corrected by a series of steps. In the incompressible form used here, it is assumed that two pressure and velocity corrections are sufficient. The first pressure correction equation of PISO is identical to that used by SIMPLE. A second corrector step is done to ensure that the continuity and momentum equations are satisfied at the end of each iteration. The second corrector step requires the solution of a second pressure correction equation, and thus the computation time per iteration will be longer for PISO than for either of the other algorithms presented here.

Due to the grid being non-orthogonal, the pressure correction equations contain cross derivatives, which lead to a nine-point formulation (ie. the pressure correction at a point P is a function of the pressure corrections at its neighbors, N, S, E, W, NE, NW, SE, and SW). For this reason it is necessary to either neglect the cross derivatives, incorporate them into the source term, or use a nine-point solver, since Shyy et al. [57] found that incorporating the cross derivative terms in the source term had no advantages over the method of neglecting the cross derivative terms. It is also reported by Ando et al. [58] that the use of a nine-point solver ensured stability and robustness of the computational method. For the reasons mentioned above, the semi-implicit solver of Peric [59] was employed in this study to solve the pressure correction equation.

3.5.3 Velocity Correction Algorithm

The Cartesian velocities U and V were corrected and contravariant velocities $\tilde{U}$ and $\tilde{V}$ were calculated using the new values of U and V rather than computing the Cartesian

velocities and correcting contravariant velocities. This is because it was found that the former method gives more accurate results and is more efficient than the latter.

The velocity correction equations for U and V are:

$$U = U^* + U' \tag{96}$$

$$V = V^* + V' \tag{97}$$

Substituting the velocity corrections U' and V':

$$U = U^* + B^u p'_\xi + C^u p'_\eta \tag{98}$$

$$V = V^* + B^v p'_\xi + C^v p'_\eta \tag{99}$$

where

$$B^u = \frac{-y_\eta}{A^u_p}; \quad B^v = \frac{x_\eta}{A^v_p}; \quad C^u = \frac{y_\xi}{A^u_p}; \quad C^v = \frac{-x_\xi}{A^v_p} \tag{100}$$

and where A^u_p and A^v_p are the coefficients of U_p and V_p, respectively. $\tilde{U}$ and $\tilde{V}$ were calculated using the definition of the contravariant velocities.

Chapter 4

Results and Discussion

This chapter presents the numerical results obtained from the modeling of turbulence phenomena in backward-facing step and jet flows.

The experimental data of Driver and Seegmiller [2] and Chandrsuda and Bradshaw [5] were used to validate the turbulence models developed in chapter 2 for backward-facing step flows while, the experimental data of Antonia et al. [8, 9, 10, 11, 12, 13] , Heskestad [14] and Gutmark and Wygnanski [16] were used to validate the model for jet flows computations.

The iterative solution procedure is terminated when the maximum value of the relative residual sources of U, V and mass balance falls below 1%. However, the computations of the triple products are terminated when the relative residual sources fall below 3×10^{-8} for $< u_i u_j u_k >$ and 5×10^{-9} for $< u_i u_j \theta >$.

The complete process of solving the momentum, temperature and related turbulence products equations takes approximately 60 minutes of CPU time on a UNIVAC 1100 computer. The CPU time varies with Reynolds number of the flow.

Figures 9 and 10 show numerical grids used in the computations of backward-facing step flow. The figures shown here are the actual computation domains used for experiments of Driver and Seegmiller and Chandrsuda and Bradshaw, respectively. These are 62×62 mesh grid system with the grid expanding linearly at the rate of 2% and 3% in the axial and transverse directions, respectively. The height of the channels are magnified five times for better visualization.

Figures 11 and 12 show the velocity variations inside the solution domain for the experiment of Driver and Seegmiller and Chandrsuda and Bradshaw, respectively.
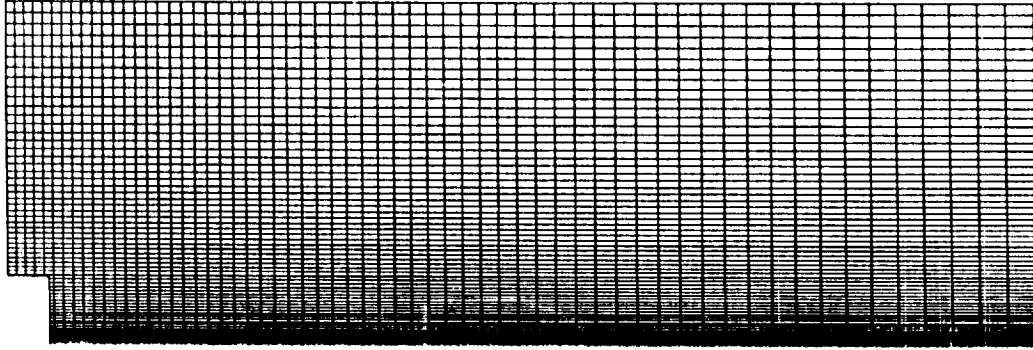
Figure 9: Grid system used in the computations of backward-facing step flow for the experiment of Driver and Seegmiller (5:1 magnification radially).
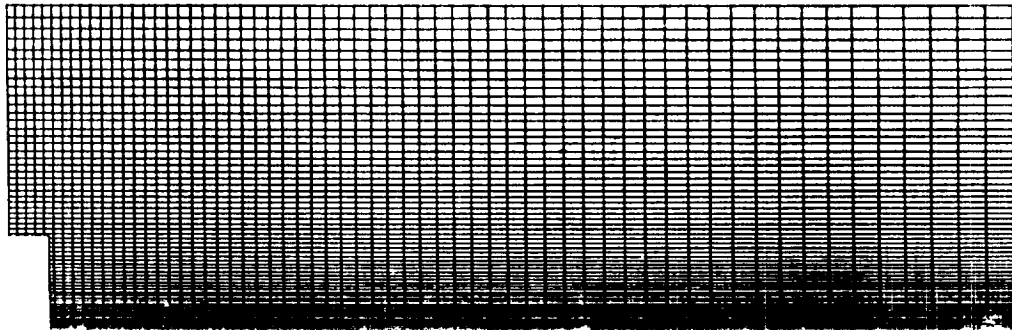

Figure 10: Grid system used in the computations of backward-facing step flow for the experiment of Chandrsuda and Bradshaw (5:1 magnification radially).
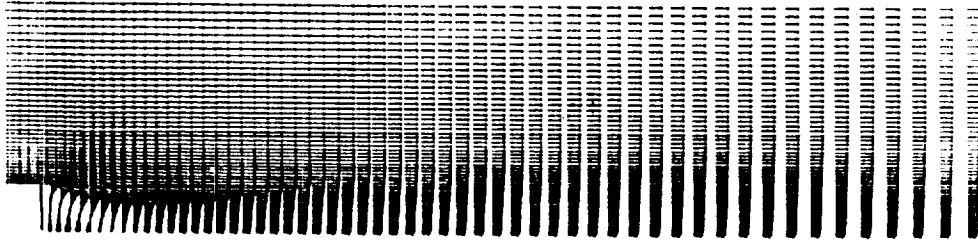
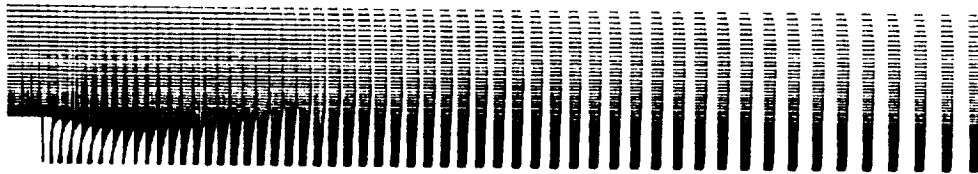Figure 11: Velocity variations inside the solution domain for the experiment of Driver and Seegmiller.

Figure 12: Velocity variations inside the solution domain for the experiment of Chandrsuda and Bradshaw.

Figures 13 and 14 show variations of the computed Reynolds stresses for the solution domain.

Figures 15 and 16 show the Low-Reynolds and high-Reynolds number model's third-moment variations, respectively. It can be seen that the high-Reynolds number model predicted higher levels at the near-wall region.

The solutions are obtained by using a 75 constant grid mesh system across the traversing direction of the jet and computations are terminated when the desired axial location is solved.

The complete process of solving the momentum, Reynolds stresses and temperature equations takes about 5 minutes of CPU time on a UNIVAC 1100 computer.

Figure 17 shows the comparisons of computational results with the measured velocity profiles of Heskestad [14], Gutmark and Wygnanski [16] and Antonia et al. [9] at self-preserving region. Figure 18 shows the comparison of the computed temperature profile with the data of Antonia et al.[9]. The agreements are very satisfactory in all three cases.

Results by Using Different Pressure-Strain Correlation Model

Figures 19 and 20 show the comparisons of computed Reynolds stresses with the experimental data of Heskestad [14] and Gutmark and Wygnanski [16]. Three different models are used, and the transport equations model with the pressure strain correlations developed here (see sec 2.3). The new model gives excellent predictions for the Reynolds stresses $< uu >$ and $< vv >$. However, this model always give higher turbulent shear stress, $< uv >$.

Comparisons of elliptic flows are shown in Figures 21 to 27. Figure 21 shows the computed mean velocity profiles and are compared with the experimental data of Chandrsuda and Bradshaw and of Driver and Seegmiller, respectively.

Figures 22 - 27 show results of the Reynolds stresses for the same cases as mentioned above. It is obseved that the new model considerably improves the predictions for all the components of the Reynolds stresses except $< vv >$. The component of $< vv >$ are underpredicted by employing the present model when compared with other models. However, it is also noticed that the experimental data for $< vv >$ are much higher in the cases of backward-facing step than those for jet flows. Thus, the predictions by the new model may be more consistent with the data of jet flows than those of step flows.
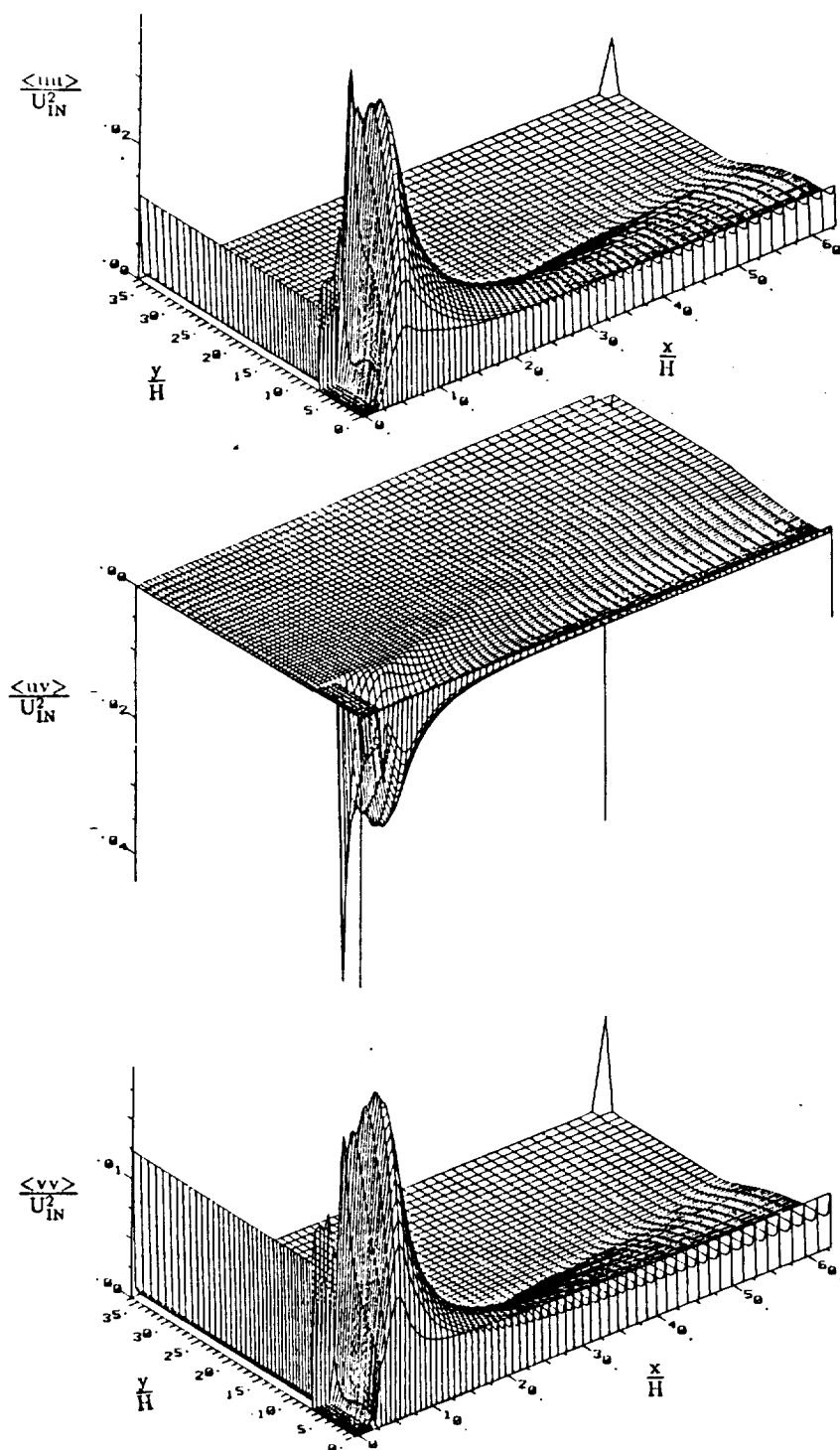
Figure 13: Reynolds stresses variations for the experiment of Driver and Seegmiller.
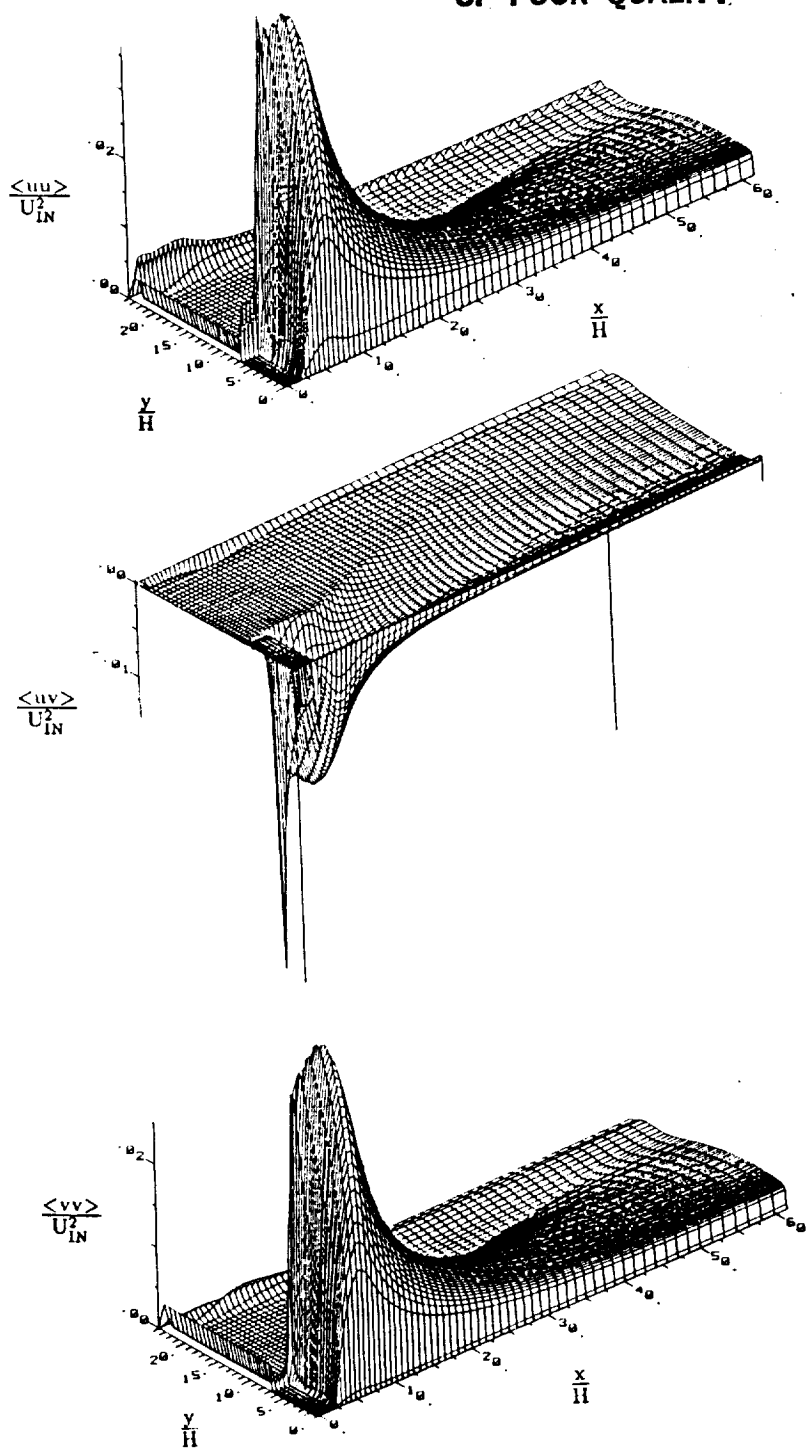
Figure 14: Reynolds stresses variations for the experiment of Chandrsuda and Bradshaw.
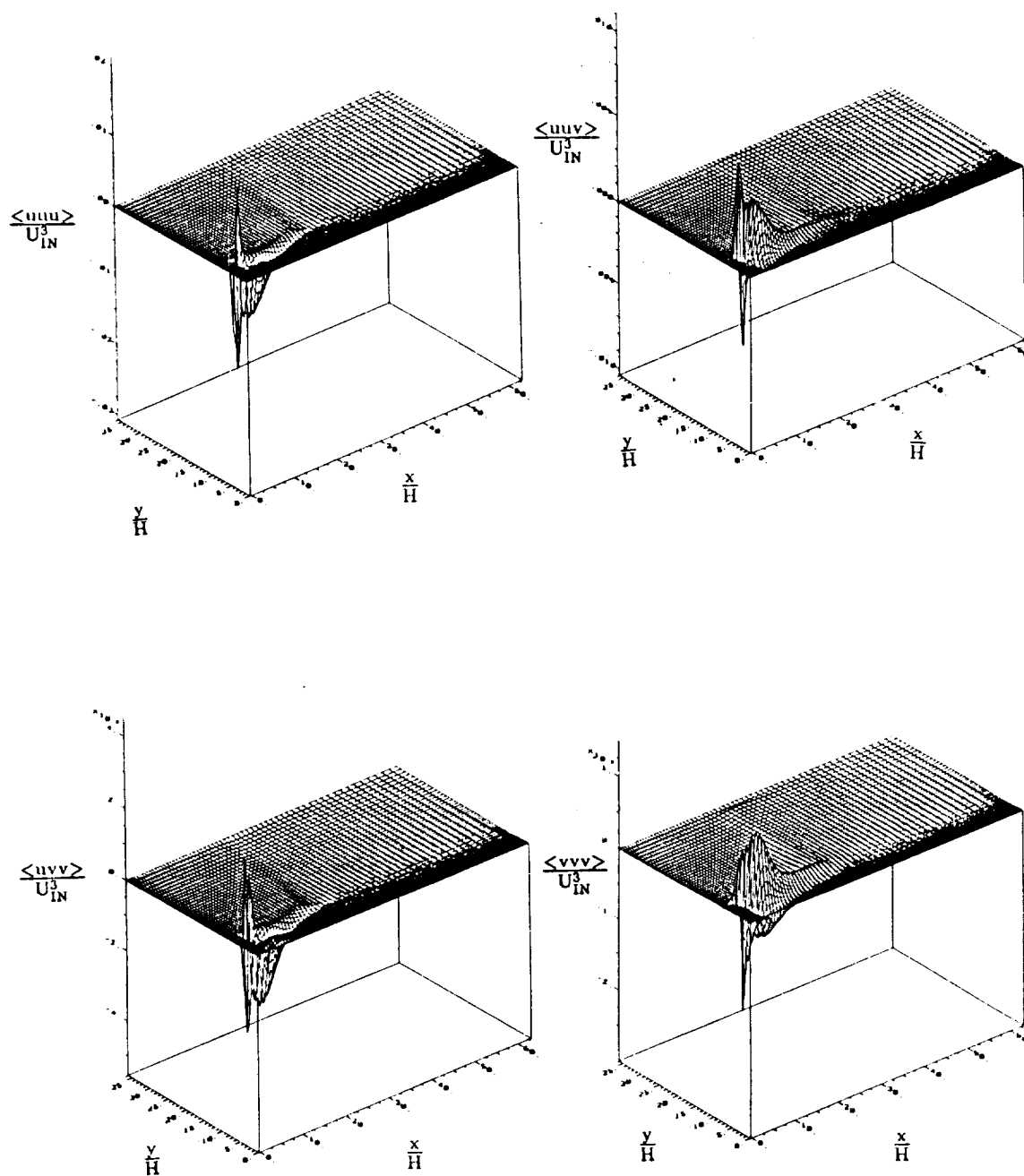
Figure 15: Low-Reynolds number third-moment variations throughout the solution domain for the data of Driver and Seegmiller.
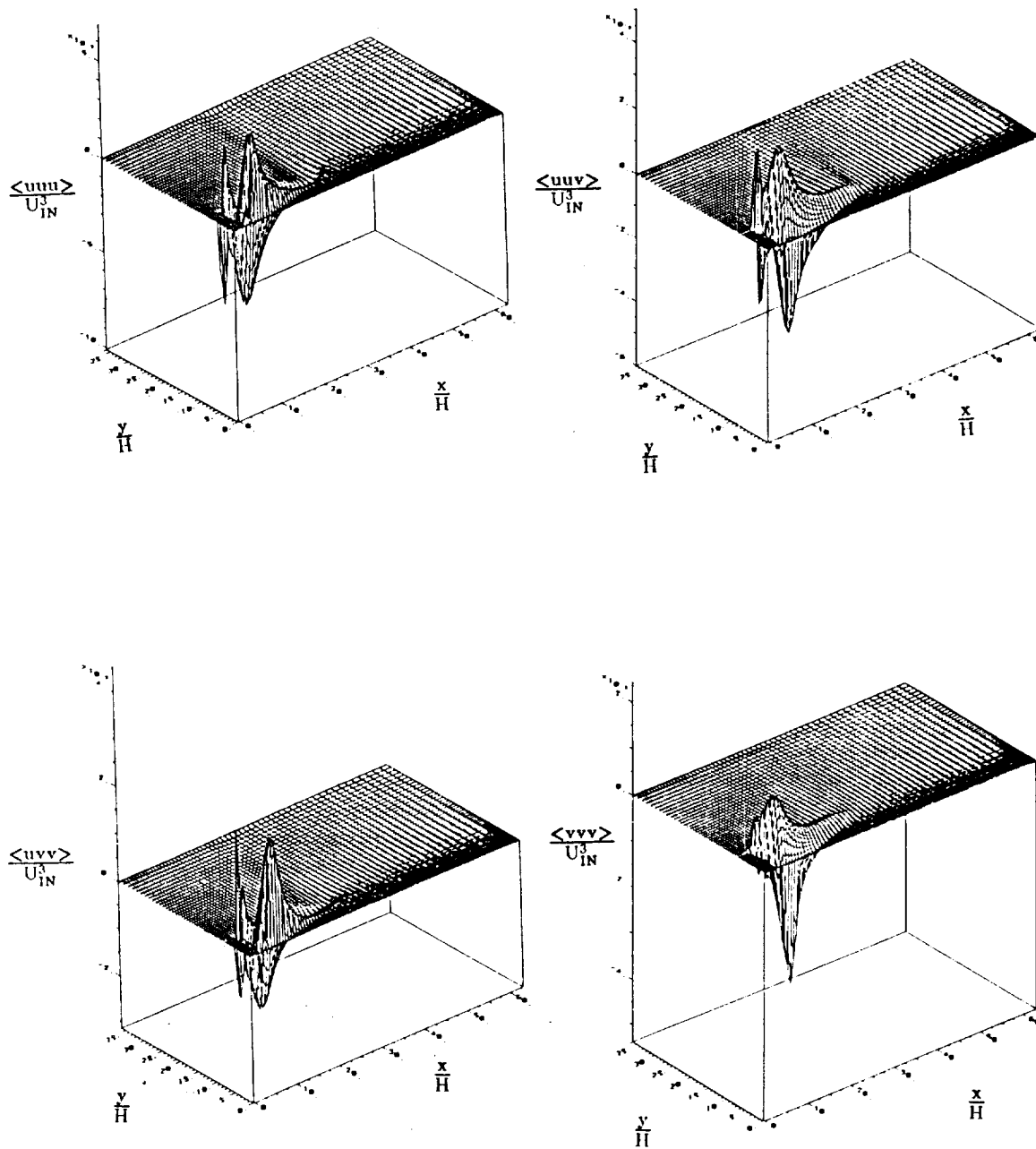
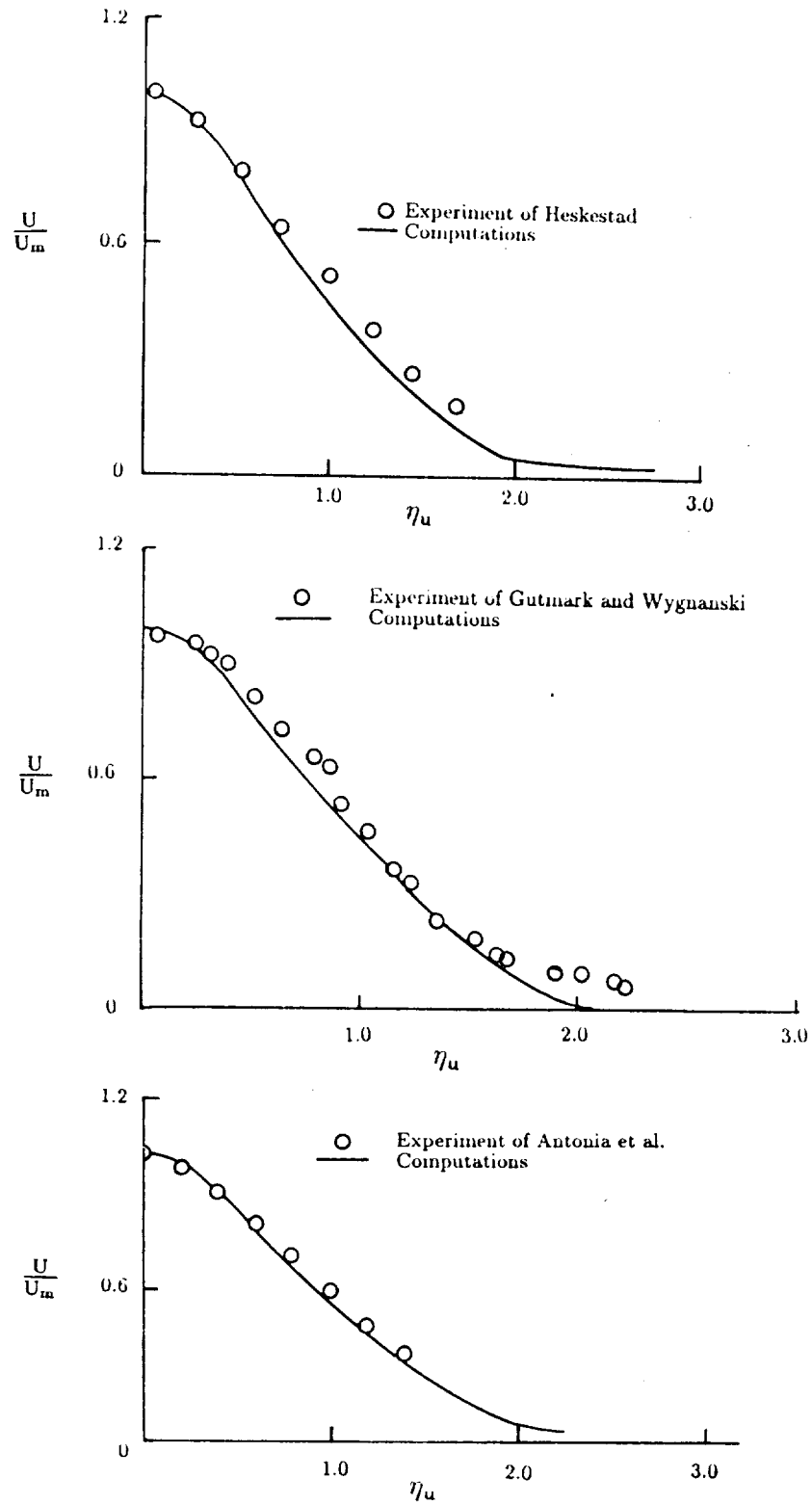Figure 16: High-Reynolds number third-moment variations throughout the solution domain for the data of Driver and Seegmiller.

Figure 17: U velocity profile - Comparison with the data of Heskestad, Gutmark and Wygnanski and Antonia et al..
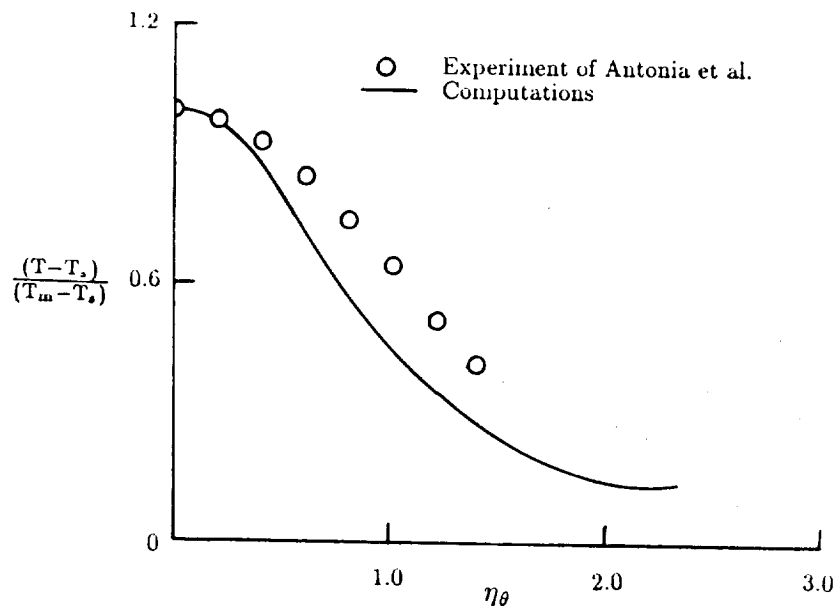
Figure 18: Temperature profile - Comparison of the computed temperature profile with the data of Antonia et al..

Flows Through Irregular Boundary Ducts

Calculations were performed for laminar flow (Re = 500) in a kidney shaped channel with a 25x32 grid using the SIMPLE, SIMPLEC, and PISO pressure correction algorithms. The calculations were considered to be converged when the normalized mass and momentum residuals were reduced to less than 0.01 %. The computed velocity vectors for the flows through the kidney shaped channel and through a diaphragm pump chamber are shown in Figure 21.

Computed velocity vectors through a 180° turn around duct is shown in Figure 22.

A comparison of the three pressure correction algorithms is shown in Figure 23. It is shown that both SIMPLEC and PISO require approximately 45 % fewer iterations than SIMPLE to meet the above mentioned convergence criteria. Since one PISO iteration takes longer to complete than either one SIMPLE or SIMPLEC iteration, comparisons were also made on the basis of work units (WU), where we define one WU to be equal to the time required to complete one SIMPLE or SIMPLEC iteration. Figure 24 shows the comparison of the three algorithms on the basis of work units. Here it is seen that PISO requires 29 % less computation time, and SIMPLEC requires
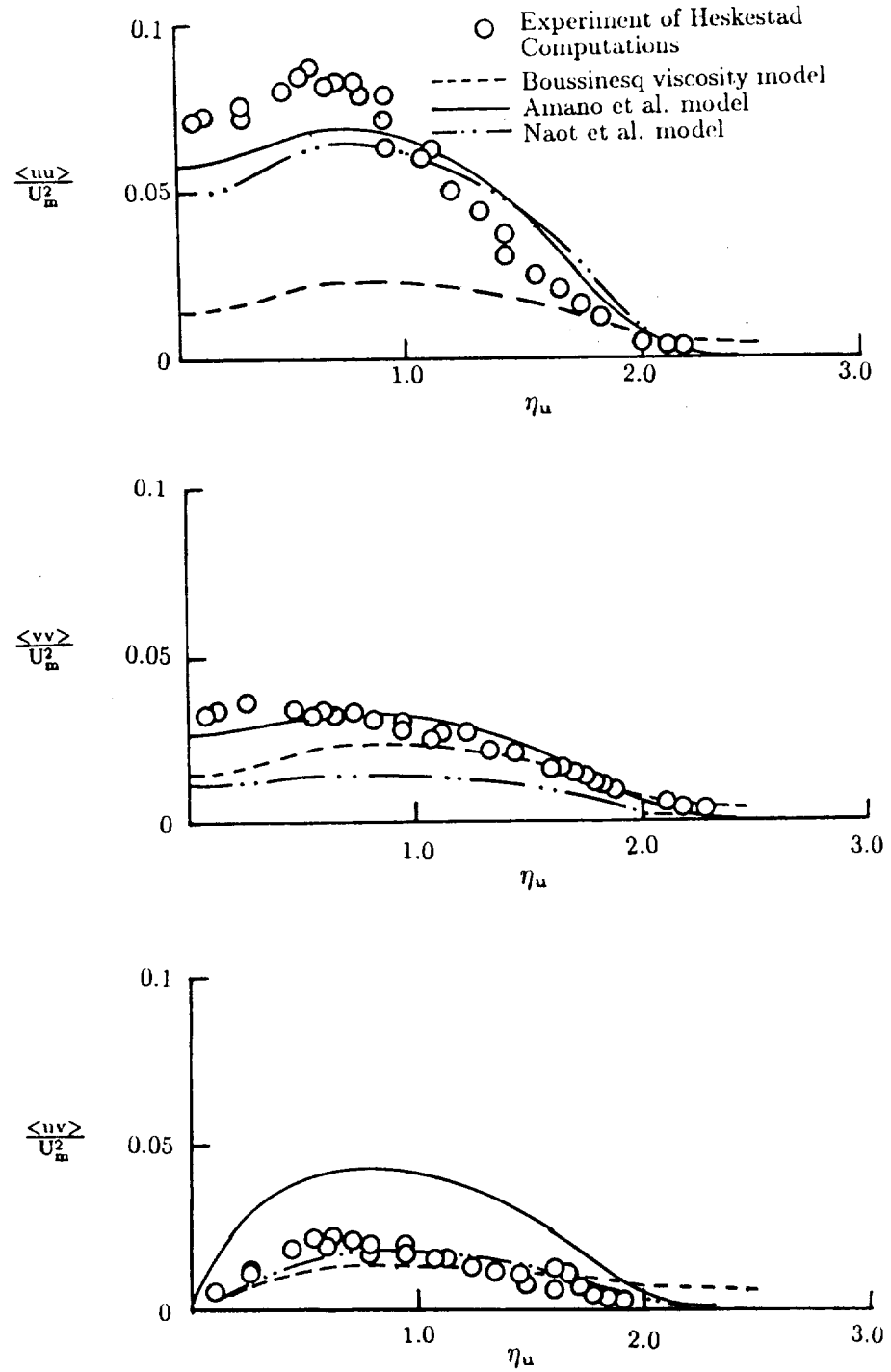
Figure 19: Reynolds-Stress profiles compared with the data of Heskestad.
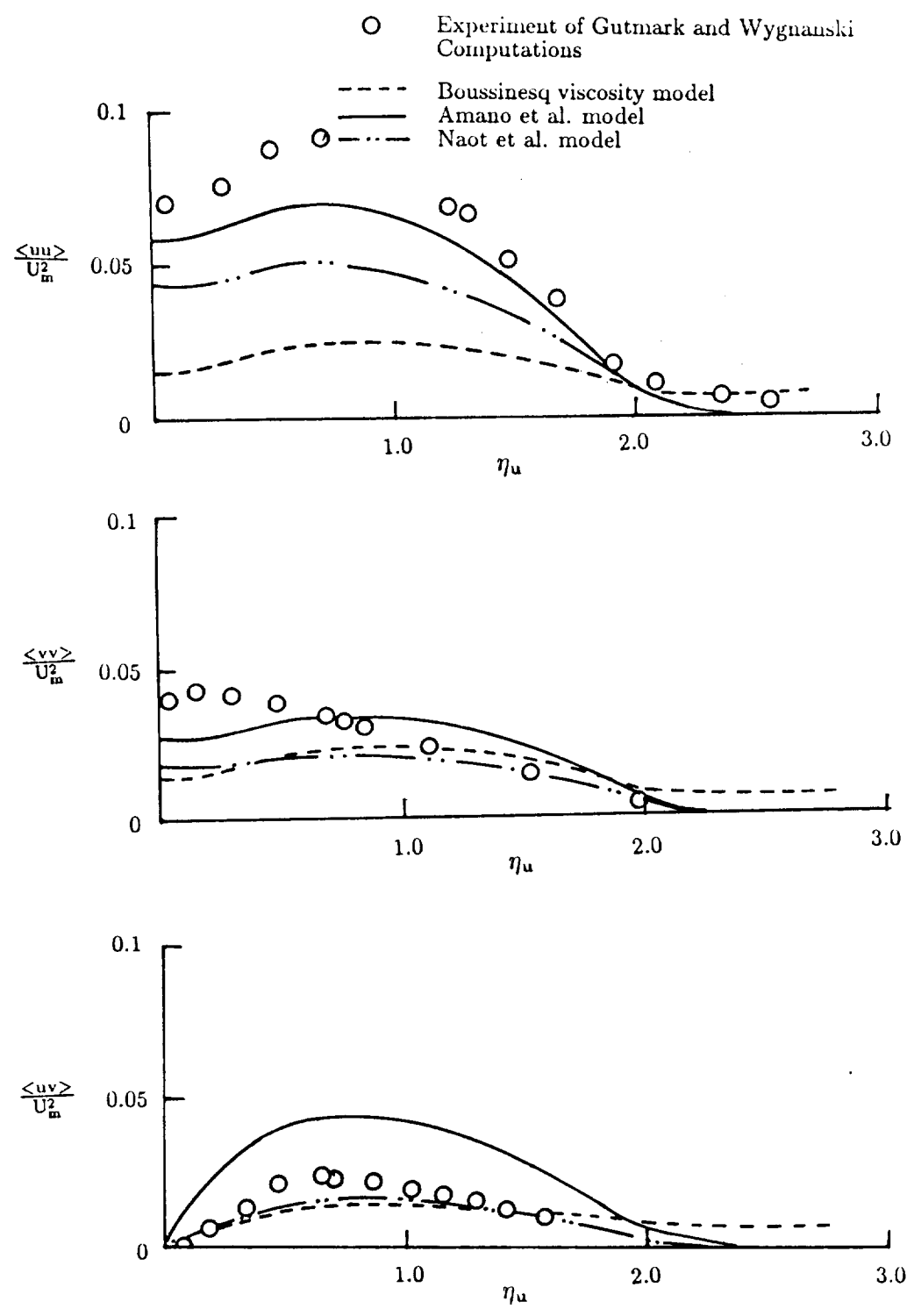
Figure 20: Reynolds-Stress profiles compared with the data of Gutmark and Wygnanski.
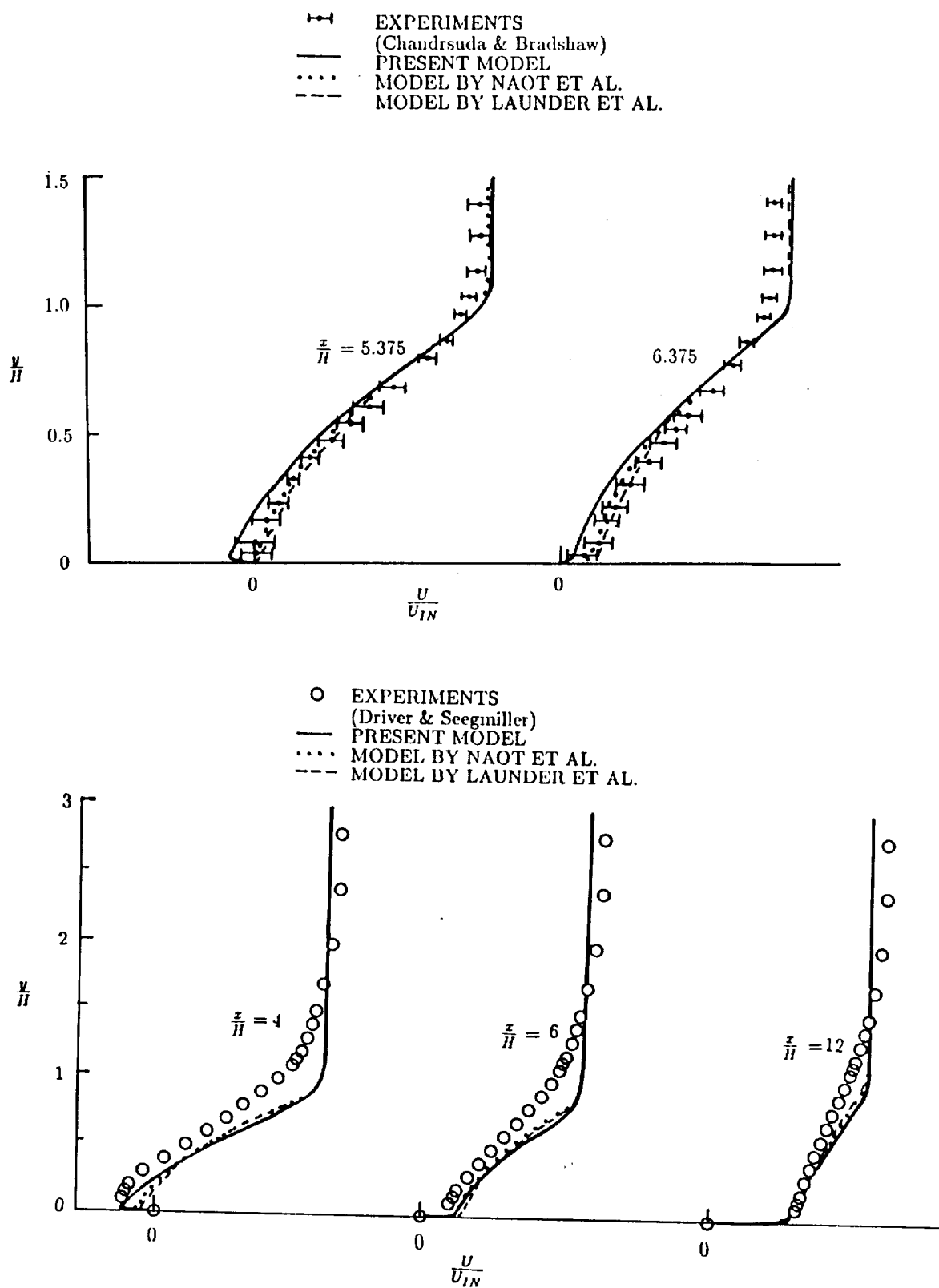
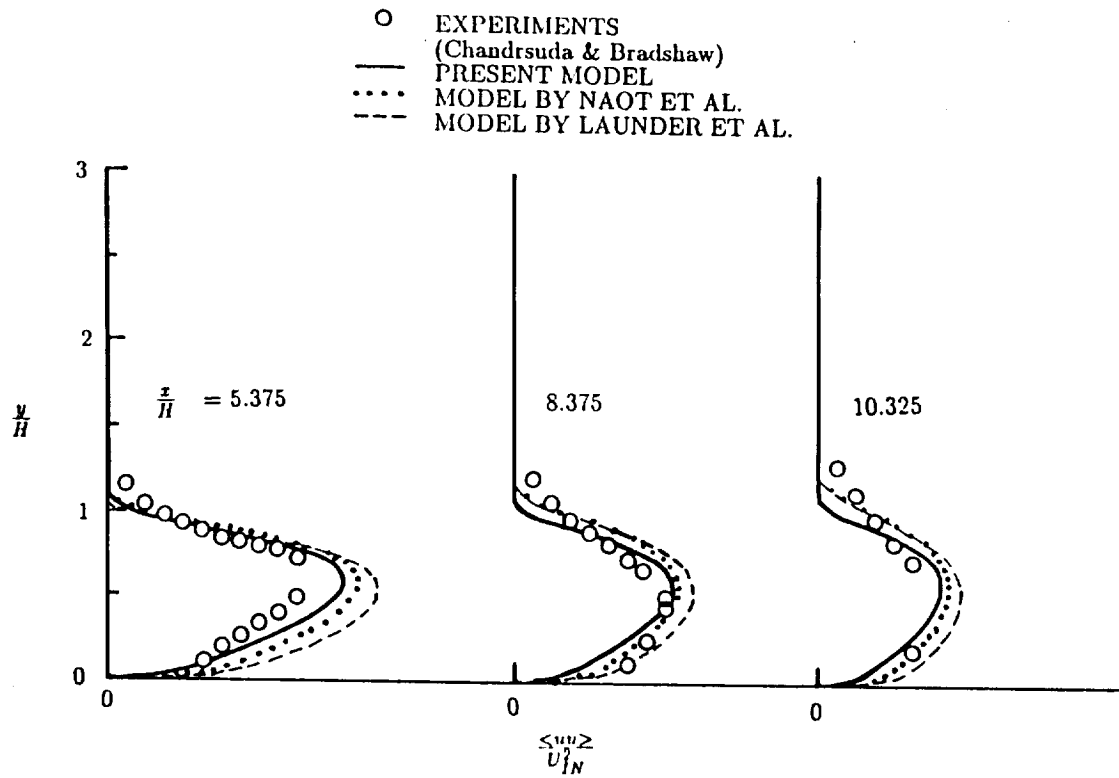Figure 21: Mean velocity profiles downstream from step.

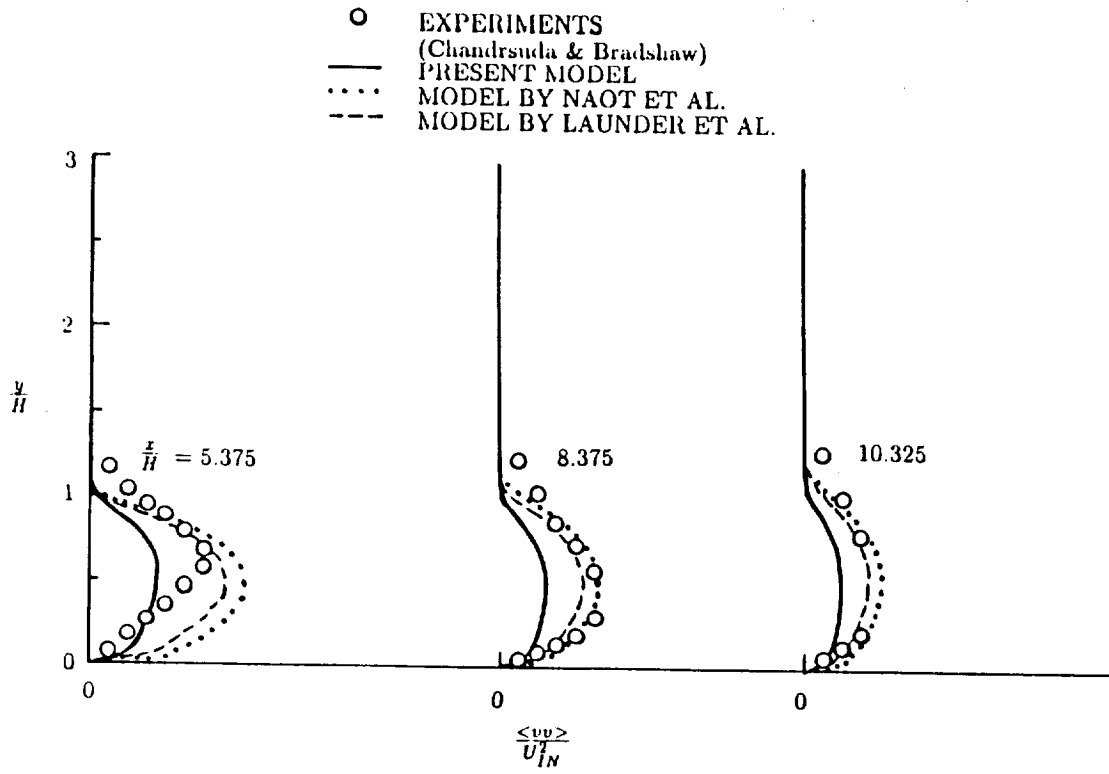Figure 22: Reynodls-stress profiles downstream from step.

Figure 23: Reynodls-stress profiles downstream from step.

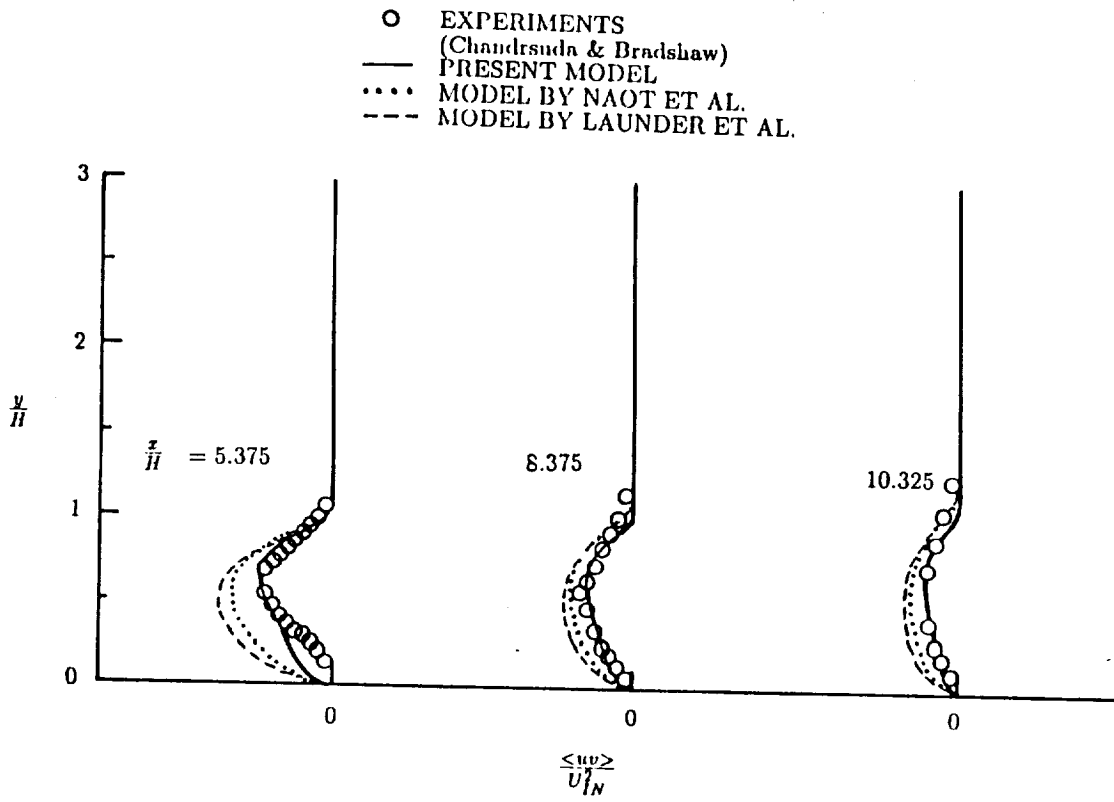Figure 24: Reynodls-stress profiles downstream from step.
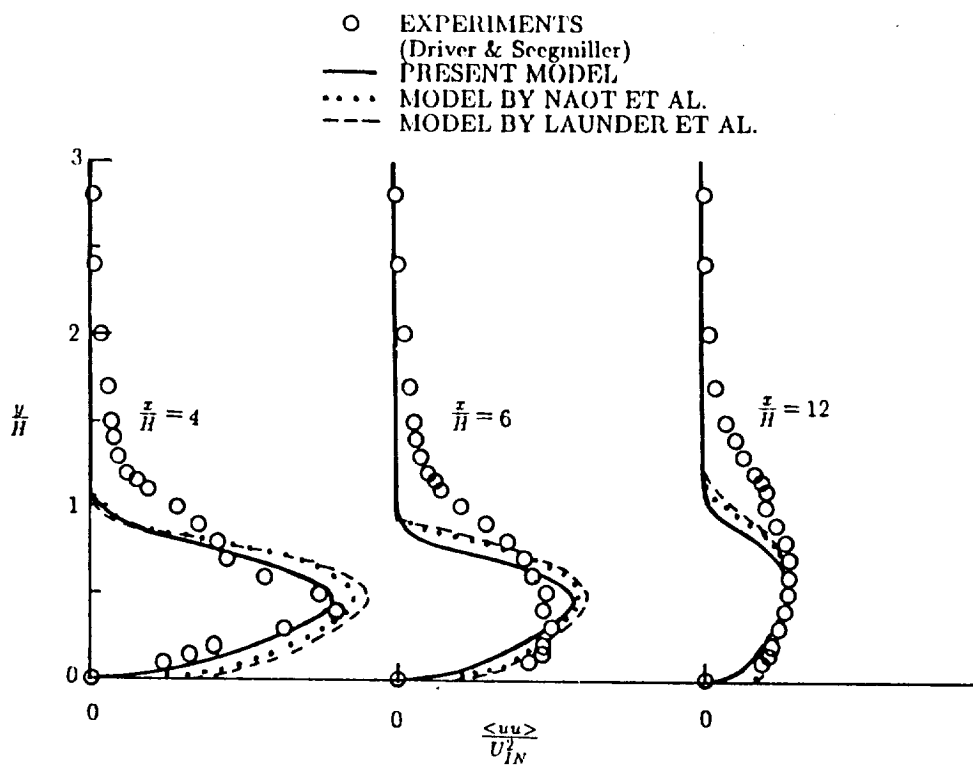
Figure 25: Reynodls-stress profiles downstream from step.
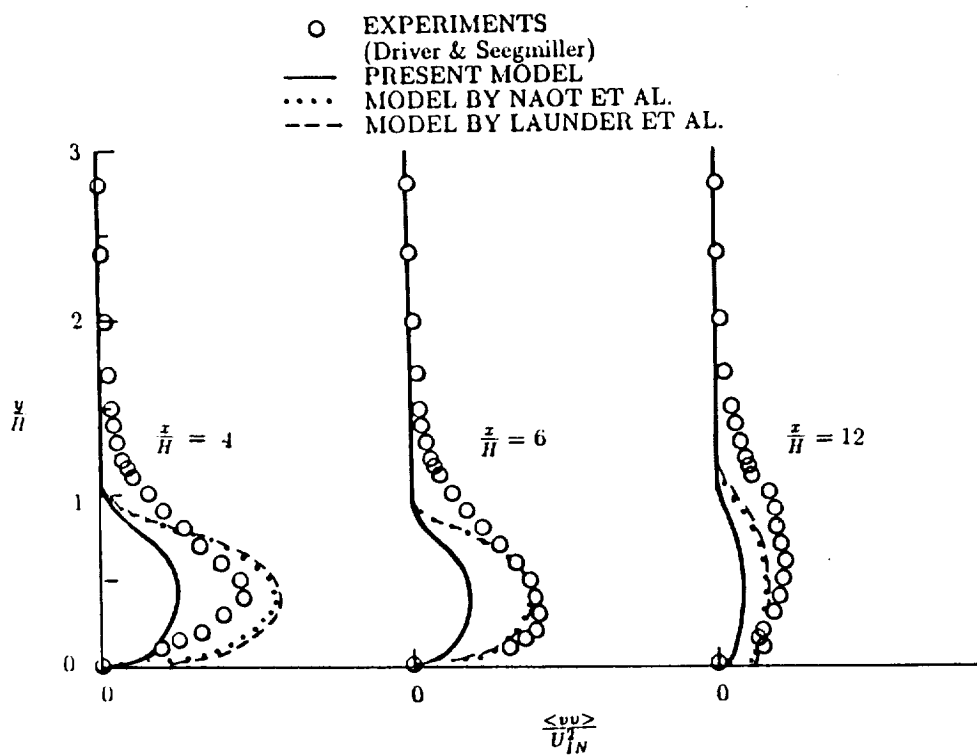
Figure 26: Reynodls-stress profiles downstream from step.
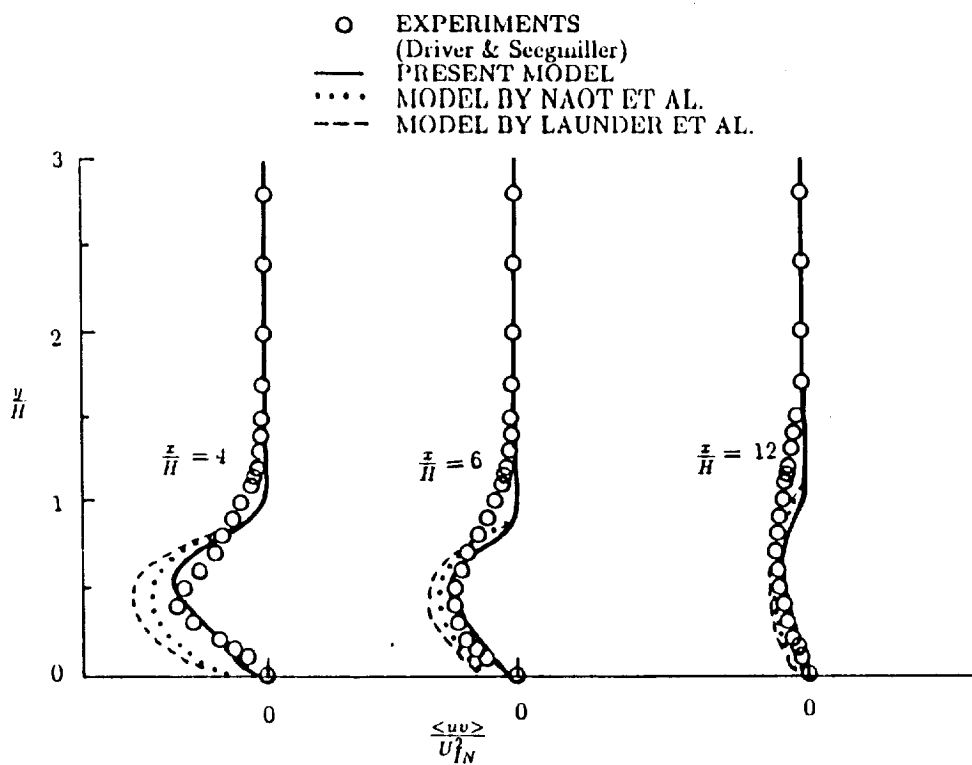
Figure 27: Reynodls-stress profiles downstream from step.
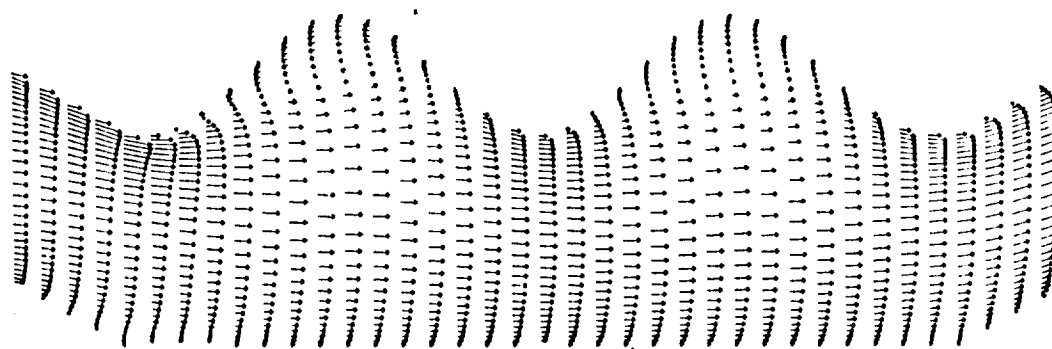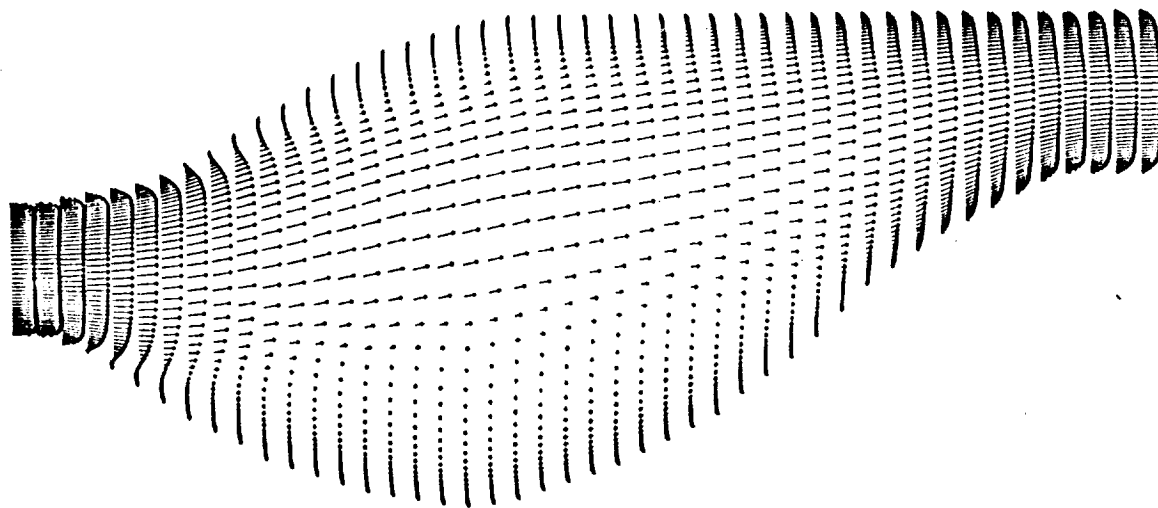
Figure 28: Velocity vectors in a kidney shaped channel (top) and in a diaphragm pump chamber (bottom)

Figure 29: Velocity vectors through a 180° turn around duct.
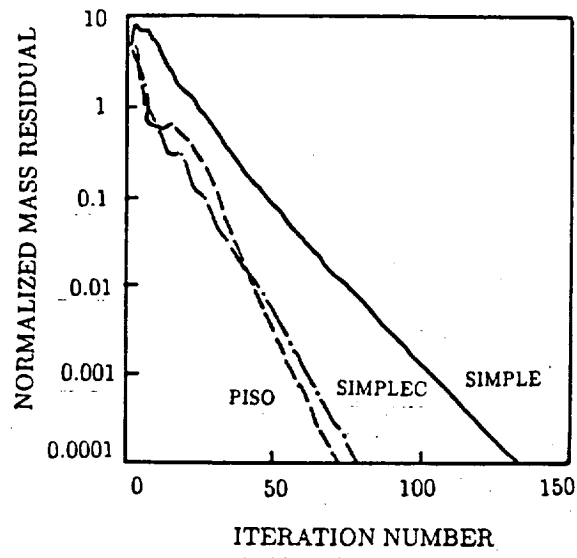
Figure 30: Comparison of three different pressure correction algorithms.

41 % less computation time than SIMPLE.
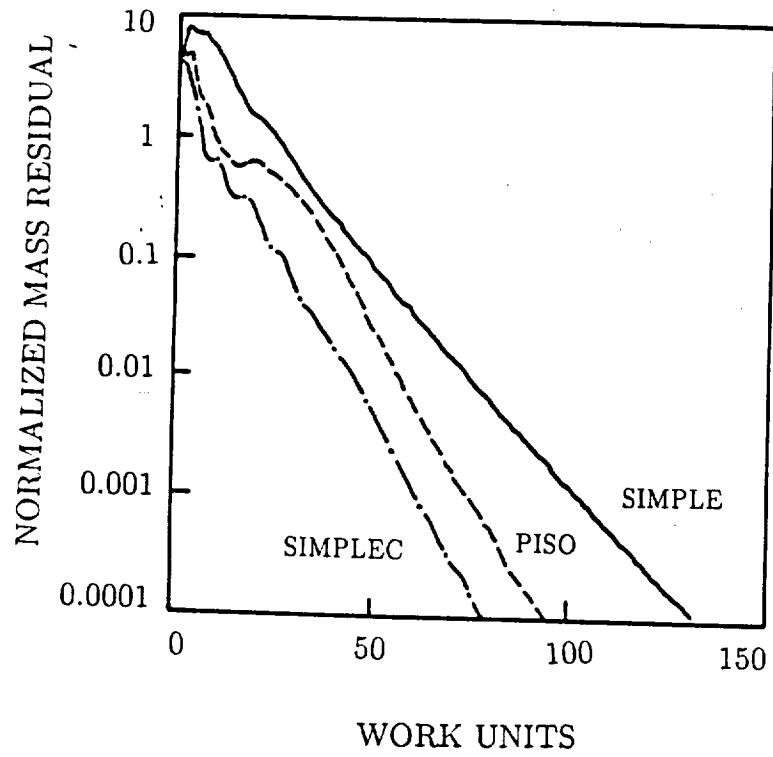
Figure 31: Comparison of three different pressure correction algorithms.

Chapter 5

Conclusions

After completing the studies presented in the previous chapters, a few observations is made and presented below.

There are a few advantages in using the full transport equations to solve turbulent flows. Presented below is a list of these advantages.

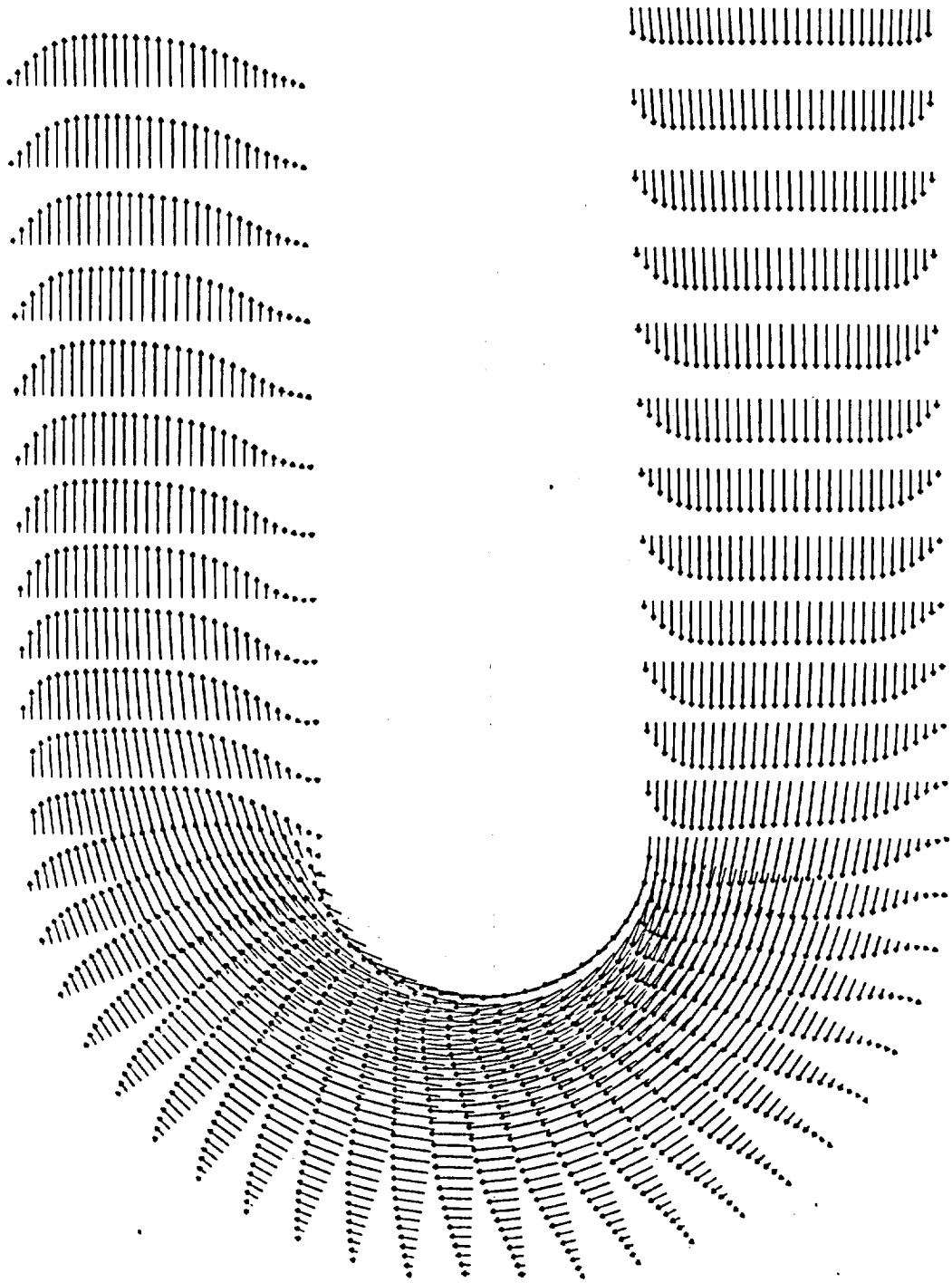1. The Reynolds-Stress model developed in this study predicts the separating and reattaching shear flows properly.

2. The transport equations for the third-moment of turbulence predicts the rapid changes of third-order turbulence velocity fluctuating tensor in the reattaching and recirculating flow regions.

3. The transport equations are more superior to the algebraic equations in the predictions of turbulence quantities because the convective and diffusive effects neglected by the algebraic models are accounted for by the transport equations.

4. The Low-Reynolds number model of third-moment of turbulence which promotes the dissipation effects of the third-moment in the near-wall region, improves the predictions of third-moment considerably and gives more universal results than the algebraic equations.

5. The newly developed parabolic code predicts the turbulent jet flows well, and further investigations and testings should be carried out to further test the abilities of this code.

6. The model predicted the mean velocity profiles to within 5% of the measured values.

7. The predictions of Reynolds stresses is very sensitve to the choice of pressure-strain correlation. Presently, the model of Amano et al. [35] produces the best predictions.

8. This code is more preferable than the code of Patankar and Spalding [31] because no coordinate transformations is needed.

9. The SIMPLEC and PISO algorithms require far fewer iterations than the SIMPLE algorithm. This shows that the "consistent" approximation used in SIMPLEC and the operator splitting approximation used in PISO are better than the assumption used in SIMPLE, namely that the velocity correction at a point is not affected by the velocity corrections of its neighbors.

10. The SIMPLEC algorithm proved to be more efficient than either PISO or SIMPLE for the case studied.

11. The PISO algorithm uses more memory than either SIMPLE or SIMPLEC, but has an advantage over the other algorithms in that it can be used for non-iterative time-dependent solutions.

12. The increased efficiency of SIMPLEC and PISO compared to SIMPLE would probably be more dramatic if a finer grid had been used, since the performance of SIMPLE degrades dramatically as the grid is refined [61].

Finally, in order to predict the turbulence quantities accurately, the solution of the full transport equations of each individual quantity is needed.

Bibliography

[1] Peterson, V.L. and Bailey, F.R., "Close to Real Life," *Aerospace America,* Vol. 26, No. 7, 1988, pp. 18-24.

[2] Driver, D. M. and Seegmiller, H. L., "Features of a Reattaching Turbulent Shear Layer in Divergent Channel Flow," *AIAA Journal,* Vol. 23, No. 2, 1985, pp. 163-171.

[3] Jones, W. P. and Launder, B. E., "The Prediction of Laminarization with a Two-Equation Model of Turbulence," *International Journal of Mass Transfer,* Vol. 15, 1972, pp. 301-314.

[4] Hutchings, B. and Iannuzzelli, R., "Taking the Measure of Fluid Dynamics Software," *Mechanical Engineering,* Vol. 109, No. 5, 1987, pp. 72-76.

[5] Chandrsuda, C. and Bradshaw, P., "Turbulence Structure of a Reattaching Mixing Layer," *Journal of Fluid Mechanics,* Vol. 110, 1981, pp. 171-194.

[6] Driver, D. M. and Seegmiller, H. L., "Features of a Reattaching Turbulent Shear Layer Subject to an Adverse Pressure Gradient," AIAA Paper 82-1029, June, 1982.

[7] Vogel, J. C. and Eaton, J. K., "Heat Transfer and Fluid Mechanics Measurements in the Turbulent Reattaching Flow Behind a Backward-Facing Step," Thermoscience Division, Department of Mechanical Engineering, Stanford University, Report MD-44, 1984.

[8] Browne, L.W.B., Antonia, R.A. and Chambers, A.J., "The Interaction Region of a Turbulent Plane Jet," *Journal of Fluid Mechanics,* Vol. 149, 1984, pp. 355-373.

[9] Antonia, R.A., Browne, L.W.B., Chambers, A.J. and Rajagopalan, S., "Budget of the Temperature Variance in a Turbulent Plane Jet," *International Journal of Heat and Mass Transfer,* Vol. 26, No. 1, 1983, pp. 41-48.

[10] Antonia, R.A., "On a Heat Transport Model for a Turbulent Plane Jet," *International Journal of Heat and Mass Transfer,* Vol. 28, No. 10, 1985, pp. 1805-1812.

[11] Browne, L.W.B. and Antonia, R.A., "Measurements of Turbulent Prandtl Number in a Plane Jet," *Journal of Heat Transfer,* Vol. 105, 1983, pp. 663-665.

[12] Antonia, R.A. and Browne, L.W.B., "The Destruction of Temperature Fluctuations in a Turbulent Plane Jet," *Journal of Fluid Mechanics,* Vol. 134, 1983, pp. 67-83.

[13] Chambers, A.J., Antonia, R.A. and Fulachier, L., "Turbulent Prandtl Number and Spectral Characteristics of a Turbulent Mixing Layer," *International Journal of Heat and Mass Transfer,* Vol. 28, No. 8, 1985, pp. 1461-1468.

[14] Heskestad, G., "Hot-Wire Measurements in a Plane Turbulent Jet," *Journal of Applied Mechanics,* Vol. 32, 1965, pp. 721-734.

[15] Everitt, K.W. and Robin, A.G., "The Development and Structure of Turbulent Plane Jets," *Journal of Fluid Mechanics,* Vol. 88, part 3, 1978, pp. 563-583.

[16] Gutmark, E. and Wygnanski, I., "The Planar Turbulent Jet," *Journal of Fluid Mechanics,* Vol. 73, part 3, 1976, pp. 465-495.

[17] Wygnanski, I and Fiedler, H., "Some Measurements in the Self-Preserving Jet," *Journal of Fluid Mechanics,* Vol. 38, part. 3, 1969, pp. 577-612.

[18] Wygnanski, I. and Fiedler, H., "The Two-Dimensional Mixing Region," *Journal of Fluid Mechanics,* Vol. 41, part. 2, 1970, pp. 327-361.

[19] Gosman, A.D., Pun, W. M., Runchal, A. K., Spalding, D. B. and Wolfshtein, M., *Heat and Mass Transfer in Recirculating Flows,* Academic Press, 1969.

[20] Pope, S. B. and Whitelaw, J. H., "The Calculation of Near-Wake Flows," *Journal of Fluid Mechanics,* Vol. 73, 1976, pp. 9-32.

[21] Schlichting, H., "Laminare Strahlausbreitung," *ZAMM* Vol. 13, 1933, pp. 260-263.

[22] Bickley, W.G., "The Plane Jet," *Philosophical magazine, Series. 7*, Vol. 23, No. 156, 1937, pp. 727-730.

[23] Goldstein, S., *Modern Development in Fluid Dynamics,* Oxford, 1943.

[24] Hanjalic, K. and Launder, B.E., "A Reynolds Stress Model of Turbulence and its Application to Thin Shear Flows," *Journal of Fluid Mechanics,* Vol. 52, part. 4, 1972, pp. 609-638.

[25] Dekeyser, I., "Numerical Prediction of an Symmetrical Heated Plane Jet with a Second-Moment Turbulence Closure," *International Journal of Heat and Mass Transfer,* Vol. 28, No. 3, 1985, pp. 653-662.

[26] Sini, J.F. and Dekeyser, I., "Numerical Prediction of Heated Turbulent Shear Flows with a Second Moment Turbulence Closure," *Proceedings International Symposium On Refined Flow Modeling and Turbulence Measurements,* The University of Iowa, Iowa City, 1985.

[27] Sini, J.F. and Dekeyser, I., "Numerical Prediction of Turbulent Plane Jets and Forced Plumes by use of the $k - \varepsilon$ model of turbulence," *International Journal of Heat and Mass Transfer,* Vol. 30, No. 9, 1987, pp. 1787-1801.

[28] Dekeyser, I. and Launder, B.E., "A comparison of Triple-Moment Temperature-Velocity Correlations in the Asymmetric Heated Jet with Alternative Closure Models," *Fourth International Symposium on Turbulent Shear Flows,* Karlsruhe, 1983.

[29] Samaraweera, D.S.A., *Turbulent Heat Transport in Two- and Three-Dimensional Temperature Fields,* Ph.D. Thesis, University of London, 1978.

[30] Launder, B. E. and Samaraweera, D. S., "Application of a Second Moment Turbulence Closure to Heat and Mass Transport in Thin Shear Flows, I. Two-Dimensional Transport," *International Journal of Heat and Mass Transfer,* Vol. 22, 1979, pp. 1631-1643.

[31] Patankar, S. V. and Spalding, D. B., *Heat and Mass Transfer in Boundary Layers,* Second Edition, Intertex Books, London, 1970. Beyond Backward-Facing Steps Using Reynolds-Stress Closure," *AIAA Journal,* Vol. 23, No. 9, 1985, pp. 1356-1361.

[32] Goel, P. and Amano, R.S., "Turbulence Energy and Diffusion Transport in a Separating and Reattaching Flow," AIAA Paper 86-1724, June, 1986.

[33] Goel, P. and Amano, R.S., "Third-Order Closure of Turbulence for the Prediction of Separating and Reattaching Flows," AIAA Paper 87-0289, January, 1987.

[34] Naot, D., Shavit, A. and Wolfshtein, M., "Two-point Correlation Model and the Redistribution of Reynolds Stress," *The Physics of Fluids,* Vol. 16, no. 6, 1973, pp.738-743.

[35] Amano, R.S., Chen, Jau-Der, and Chai, J. C., "Improvement of the Reynolds-Stress Model by the Pressure-Strain Correlation," to be presented at ASME Winter Annual Meeting, Chicago, 1988.

[36] Launder, B. E., Reece, G. J. and Rodi, W., "Progress in the Development of a Reynolds-Stress Turbulence Closure," *Journal of Fluid Mechanics,* Vol. 68, part. 3, 1975, pp. 537-566.

[37] Amano, R.S., Goel, P. and Chai, J.C., "Turbulence Energy and Diffusion Transport of Third-Moments in a Separating and Reattaching Flow," *AIAA Journal,* Vol. 26, No. 3, 1988, pp. 273-282.

[38] Amano, R.S. and Chai, J.C., "Transport models of the Turbulent Velocity-Temperature Product for Computations of Recirculating Flows," *Numerical Heat Transfer,* Vol. 14, No. 1, 1988, pp. 75-95.

[39] Launder, B. E., "Heat and Mass Transport," in *Turbulence - Topics on Applied Physics,* (edited by Bradshaw, P.), Vol. 12, Chapter 6, 1976.

[40] Amano, R.S. and Chai, J.C., "Transport Models of the Turbulent Velocity-Temperature Products for Computations of Recirculating Flows," ASME Proceedings of the 1988 National Heat Transfer Conference, Houston, Texas, Vol. 3, 1988, pp. 493-500.

[41] Chou, P. Y., "On Velocity Correlations and the Solutions of the Equations of Turbulent Fluctuation," *Quarterly Applied Mathematics*, Vol. 3, 1945, p. 38.

[42] Rotta, J. C., "Statistische Thearie Nichthomogener Trubulenz," *Z. Phys*, Vol. 129, 1951, p. 547.

[43] Launder, B. E., Reece, G. J. and Rodi, W., "Progress in the Development of a Reynolds-Stress Turbulence Closure," *Journal of Fluid Mechanics,* Vol. 16, no. 6, 1973, pp. 738-743.

[44] Champagne, F. H., Harris, V. G. and Corrsin, S., "Experiments on Nearly Homogeneous Turbulent Shear Flow," *Journal of Fluid Mechanics,* Vol. 41, 1970, pp. 81-139.

[45] Daly, B.J. and Harlow, F.H.,"Transport Equations in Turbulence," *The Physics of Fluids,* Vol. 13, No. 11, 1970, pp.2634-2649.

[46] Shir, C.C., "A Preliminary Numerical Study of Atmospheric Turbulent Flows in the Idealized Planetary Boundary Layer," *Journal of Atmospheric Science,* Vol. 30, 1973, pp.1327-1339.

[47] Kays, W.M. and Crawford, M.E., *Convective Heat and Mass Transfer,* McGraw Hill, Second Edition, 1980.

[48] Patankar, S. V., *Numerical Heat Transfer and Fluid Flow,* McGraw-Hill, 1980

[49] Patankar, S. V., "A Calculation Procedure for Two-Dimensional Elliptic Situations," *Numerical Heat Transfer,* Vol. 4, 1981, pp. 409-425.

[50] Spalding, D. B., "A Novel Finite-Difference Formulation for Differential Expressions Involving Both First and Second Derivatives," *International Journal for Numerical Methods in Engineering,* Vol. 4, 1972, p.551.

[51] Amano, R. S., "Development of a Turbulence Near-Wall Model and its Application to Separated and Reattached Flows," *Numerical Heat Transfer,* Vol. 7, 1984, pp. 59-75.

[52] Amano, R.S., *Numerical Study of a Turbulent Jet Impinging on a Flat Plate and Flowing into an Axisymmetric Cavity,* Ph.D. Thesis, University of California-Davis, Davis, 1980.

[53] Amano, R.S., *Finite Difference Method for Engineering,* lecture notes, University of Wisconsin-Milwaukee, Milwaukee, 1988.

[54] Amano, R.S. and Chai, J.C., "A Closure Model of Diffusion Transport of the Reynolds-Stress Equations and Its Application to a Turbulent Step Flow," *Proceedings of the Second International Symposium on Transport Phenomena in Turbulent Flows,* October 1987, Tokyo, Japan.

[55] Van Doormaal, J. P. and Raithby, G. D., " Enhancements of the SIMPLE Method for Predicting Incompressible Fluid Flows," *Numerical Heat Transfer,* Vol. 7, 1984, pp. 147-163.

[56] Issa, R. I., "Solution of the Implicitly Discretized Fluid Flow Equations by Operator-Splitting," *Journal of Computational Physics,* Vol. 62, 1985, pp. 40-65.

[57] Shyy, W., Tong, S. S. and Corea, S. M., "Numerical Recirculating Flow Calculation Using a Body-Fitted Coordinate System," *numerical Heat Transfer,* Vol. 8, 1985, pp. 99-113.

[58] Ando, Y., Kawai, M., Sato, Y. and Toh, H., "Numerical Calculations of Turbulent Flows in a Dump Diffuser," *AIAA Paper* 86-1656, 1986.

[59] Peric, M., "Efficient Semi-Implicit Solving Algorithm for Nine-Diagonal Coefficient Matrix," *Numerical Heat Transfer,* Vol. 11, 1987, pp. 251-279.

[60] Maruszewski, J. P. and Amano, R. S., "A Study of Turbulent Flow Computations in an Angled Duct With a Step," ASME Winter Annual Meeting, Chicago, 1988.

[61] Hutchinson, B. R., Galpin, P. F. and Raithby, G. D., "Application of Additive Correction Multigrid to the Coupled Fluid Flow Equations," *Numerical Heat Transfer,* Vol. 13, 1987, pp. 133-147.